Geoscience Frontiers xxx (xxxx) xxx

HOSTED BY

Contents lists available at ScienceDirect

Geoscience Frontiers

journal homepage: www.elsevier.com/locate/gsf

Research Paper

A large epeiric methanogenic Bambuí sea in the core of Gondwana supercontinent?

Sergio Caetano-Filho [a,*], Pierre Sansjofre [b], Magali Ader [c], Gustavo M. Paula-Santos [d], Cristian Guacaneme [a], Marly Babinski [a], Carolina Bedoya-Rueda [a], Matheus Kuchenbecker [e], Humberto L.S. Reis [f], Ricardo I.F. Trindade [g]

[a] Universidade de São Paulo, Instituto de Geociências, Rua do Lago, 562 – São Paulo, 05508-080, Brazil
[b] MNHN, Sorbonne Université, CNRS UMR 7590, Institut de Minéralogie, de Physique des Matériaux et de Cosmochimie, 75005, Paris, France
[c] Université de Paris, Institut de Physique du Globe de Paris, CNRS, F-75005, Paris, France
[d] Universidade Estadual de Campinas, Instituto de Geociências, Rua Carlos Gomes, 250 – Campinas, 13083-855, Brazil
[e] Universidade Federal dos Vales do Jequitinhonha e Mucuri, Instituto de Ciência e Tecnologia, Laboratório de Estudos Tectônicos, Rodovia MGT 367, Km 583 – Diamantina, 39100-000, Brazil
[f] Universidade Federal de Ouro Preto, Departamento de Geologia-Escola de Minas, Laboratório de Modelagem Tectônica, Campus Morro do Cruzeiro – Ouro Preto, 35400-000, Brazil
[g] Universidade de São Paulo, Instituto de Astronomia, Geofísica e Ciências Atmosféricas, Rua do Matão, 1226 – São Paulo, 05508-090, Brazil

ARTICLE INFO

Handling Editor: Richard M Palin

Keywords:
Methanogenesis
Ediacaran
Cambrian
Carbon isotopes
São Francisco Basin
Bambuí Group

ABSTRACT

Carbon isotope compositions of both sedimentary carbonate and organic matter can be used as key proxies of the global carbon cycle and of its evolution through time, as long as they are acquired from waters where the dissolved inorganic carbon (DIC) is in isotope equilibrium with the atmospheric CO_2. However, in shallow water platforms and epeiric settings, the influence of local to regional parameters on carbon cycling may lead to DIC isotope variations unrelated to the global carbon cycle. This may be especially true for the terminal Neoproterozoic, when Gondwana assembly isolated waters masses from the global ocean, and extreme positive and negative carbon isotope excursions are recorded, potentially decoupled from global signals. To improve our understanding on the type of information recorded by these excursions, we investigate the paired $\delta^{13}C_{carb}$ and $\delta^{13}C_{org}$ evolution for an increasingly restricted late Ediacaran-Cambrian foreland system in the West Gondwana interior: the basal Bambuí Group. This succession represents a 1st-order sedimentary sequence and records two major $\delta^{13}C_{carb}$ excursions in its two lowermost lower-rank sequences. The basal cap carbonate interval at the base of the first sequence, deposited when the basin was connected to the ocean, hosts antithetical negative and positive excursions for $\delta^{13}C_{carb}$ and $\delta^{13}C_{org}$, respectively, resulting in $\Delta^{13}C$ values lower than 25‰. From the top of the basal sequence upwards, an extremely positive $\delta^{13}C_{carb}$ excursion is coupled to $\delta^{13}C_{org}$, reaching values of +14‰ and −14‰, respectively. This positive excursion represents a remarkable basin-wide carbon isotope feature of the Bambuí Group that occurs with only minor changes in $\Delta^{13}C$ values, suggesting change in the DIC isotope composition. We argue that this regional isotopic excursion is related to a disconnection between the intrabasinal and the global carbon cycles. This extreme carbon isotope excursion may have been a product of a disequilibria between the basin DIC and atmospheric CO_2 induced by an active methanogenesis, favored by the basin restriction. The drawdown of sulfate reservoir by microbial sulfate reduction in a poorly ventilated and dominantly anoxic basin would have triggered methanogenesis and ultimately methane escape to the atmosphere, resulting in a ^{13}C-enriched DIC influenced by methanogenic CO_2. Isolated basins in the interior of the Gondwana supercontinent may have represented a significant source of methane inputs to the atmosphere, potentially affecting both the global carbon cycle and the climate.

* Corresponding author.
E-mail address: sergio.caetano.filho@usp.br (S. Caetano-Filho).
Peer-review under responsibility of China University of Geosciences (Beijing).

https://doi.org/10.1016/j.gsf.2020.04.005
Received 3 September 2019; Received in revised form 29 January 2020; Accepted 7 April 2020
Available online xxxx

Please cite this article as: Caetano-Filho, S. et al., A large epeiric methanogenic Bambuí sea in the core of Gondwana supercontinent?, Geoscience Frontiers, https://doi.org/10.1016/j.gsf.2020.04.005

1. Introduction

Major carbon isotope excursions during the Neoproterozoic Era have been interpreted in terms of global perturbation of carbon cycle (e.g. Halverson et al., 2005; Sansjofre et al., 2011), diagenetic overprint (Knauth and Kennedy, 2009; Derry, 2010), and regional perturbation of carbon cycle (e.g. Ader et al., 2009; Cui et al., 2018; Uhlein et al., 2019). Perturbations in the global carbon cycle were proposed to be driven by changes in organic matter burial rates (f_{org}), methane oxidation events, the proportion of authigenic carbonate precipitation, and oxidation of a large DOC reservoir (e.g. Rothman et al., 2003; Halverson et al., 2009; Schrag et al., 2013). During the Cryogenian and Ediacaran, the generally high $\delta^{13}C_{carb}$ values are most commonly interpreted as resulting from enhanced organic matter burial at the global scale leading to a second major oxygenation event in the Earth's history, the Neoproterozoic Oxygenation Event (Och and Shield Zhou, 2012). This large positive isotopic excursion over tens of millions of years is punctuated by rapid negative excursions associated with major glacial events (Halverson et al., 2009 and references therein).

Despite the rich carbon isotope record for Neoproterozoic basins worldwide, the identification of local to regional effects on the marine carbon cycle in these basins are rarely considered (e.g. Ader et al., 2009; Cui et al., 2018). Regional to local parameters may be particularly critical to DIC isotope composition from shallow platforms, epeiric seas and restricted basins, resulting in secular changes in carbon isotope compositions from carbonate sediments decoupled from the global carbon cycle (e.g. Fanton and Holmden, 2007; Swart, 2008; Geyman and Maloof, 2019). Such geotectonic scenarios were common during the assembly of the West Gondwana supercontinent at the Ediacaran-Cambrian transition, when large epicontinental marine basins were developed completely or partially isolated from the global ocean, such as those represented by Otavi and Bambuí groups, in São Francisco-Congo craton (e.g. Paula-Santos et al., 2017; Cui et al., 2018). In particular, the Ediacaran-Cambrian Bambuí Group, São Francisco Basin (central-east Brazil) represents a foreland system formed during Brasiliano/Pan-African orogenic cycle, in a geotectonic setting progressively surrounded by fold-thrust belts (Reis et al., 2016). This unit records an extreme positive $\delta^{13}C_{carb}$ excursion across the basin, reaching up to +16‰ (e.g. Iyer et al., 1995, Fig. 1 A), which is anomalously high with respect to the signal of other time-equivalent successions worldwide (e.g., Halverson et al., 2009). This excursion has been referred to as the Middle Bambuí Excursion (MIBE; Uhlein et al., 2019), and is associated with the sequence boundary between the two lowermost sequences from the Bambuí Group (Caetano-Filho et al., 2019).

Although several authors interpreted the MIBE as a result from the progressive restriction of the basin in the very core of Gondwana supercontinent (Iyer et al., 1995; Paula-Santos et al., 2017; Caetano-Filho et al., 2019; Uhlein et al., 2019), the mechanism behind these very high ^{13}C-enrichment remains poorly constrained. Here we present new organic carbon isotope data ($\delta^{13}C_{org}$) on three sections of the Bambuí Group from different sectors of the basin for which carbonate carbon isotope data ($\delta^{13}C_{carb}$) and a basin-wide sequence stratigraphy framework are already available (Reis and Suss, 2016; Caetano-Filho et al., 2019). We use the paired $\delta^{13}C_{org}$ and $\delta^{13}C_{carb}$ data to provide additional constraints on the mechanisms behind the ^{13}C-enrichments in these deposits and their implication for the local and global environmental conditions during the Ediacaran-Cambrian transition.

2. Geological setting

In western South America, São Francisco craton represents one of the inner and stable part of one of the paleocontinents involved in the assembly of Gondwana, by the end of Neoproterozoic Era (e.g., Heilbron et al., 2017). During these diachronous collisional events, several orogenic belts evolved around the craton, giving rise to a complex foreland system in its interior, recorded in the rocks of the Bambuí Group (e.g. Reis et al., 2016).

The Bambuí Group encompasses the basal diamictite of the Carrancas Formation which is overlain by mixed carbonate-siliciclastic deposits from Sete Lagoas, Serra de Santa Helena, Lagoa do Jacaré, Serra da

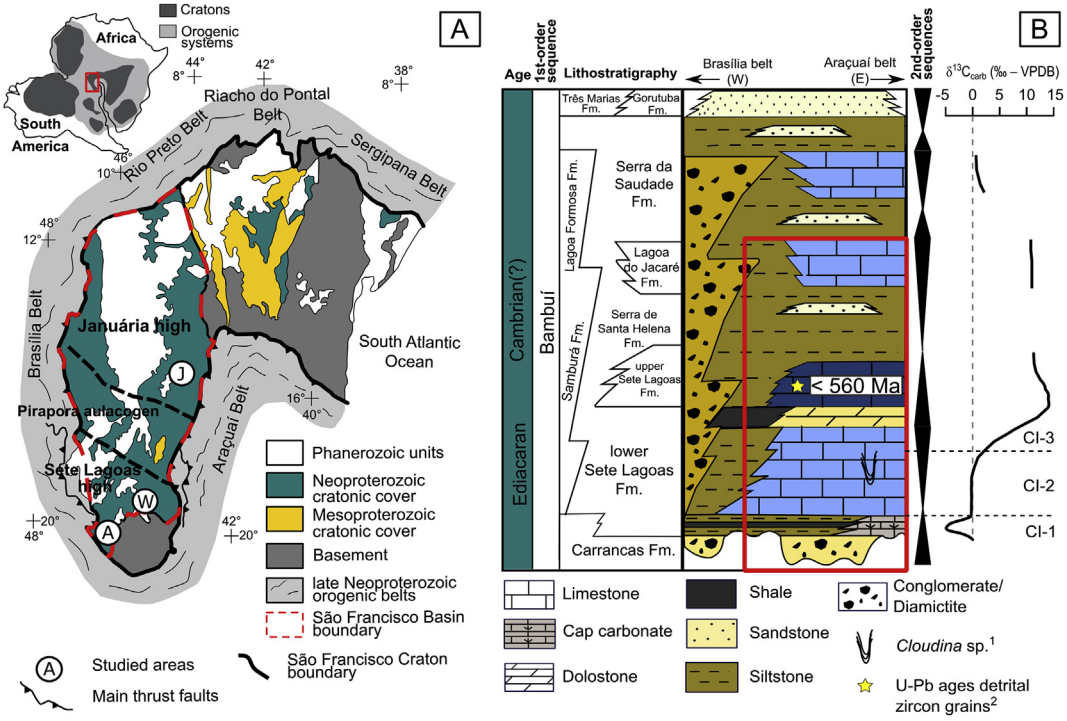

Fig. 1. (A) São Francisco Craton geological map (modified from Alkmim et al., 2006 and Reis et al., 2016). Studied sections: A – Arcos; W – Well 1; and J – Januária. (B) Stratigraphic chart from the Bambuí Group (after Reis et al., 2016). [1]Fossil occurrence from Warren et al. (2014); [2]Age from Paula-Santos et al. (2015). Carbon isotope evolution based on Paula-Santos et al. (2017), Caetano-Filho et al. (2019) and Uhlein et al. (2019). The red rectangle marks the studied interval.

Saudade and Três Marias formations (Fig. 1B). These lithostratigraphic units correspond to the most expressive strata exposed in the southern São Francisco Craton (i.e., the intracratonic São Francisco basin) and record a 1st-order foreland basin cycle (Fig. 1A and B; for a detailed review see Reis et al., 2016). We focus here on the lower to middle sedimentary successions of the Bambuí Group. These successions comprise two basin-wide and transgressive-regressive 2nd-order sequences that record major changes in the carbon isotope record (e.g. Caetano-Filho et al., 2019; Uhlein et al., 2019).

The basal 2nd-order sequence unconformably overlies Archean/Paleoprtoerozoic basement assemblages and Paleoproterozoic to early Neoproterozoic sedimentary successions of the São Francisco Basin (Reis et al., 2016). Its basal portion marks a transgressive systems tract (TST), which is composed of coarse-grained siliciclastic deposits of the Carrancas Formation grading upward into cap carbonate rocks of the basal Sete Lagoas Formation (e.g. Vieira et al., 2007; Paula-Santos et al., 2015, 2017; Kuchenbecker et al., 2016; Reis and Suss, 2016). The basal cap carbonate displays a typical negative $\delta^{13}C_{carb}$ excursion extending to −5‰ that recovers upsection to values near 0‰. The cap carbonate interval encompasses dolostones and limestones with several layers of aragonite pseudomorphs and barite crystal fans (Babinski et al., 2007; Vieira et al., 2007; Kuchenbecker et al., 2016; Okubo et al., 2018; Crockford et al., 2019). The TST are overlain by mixed carbonate-siliciclastic deposits of the middle Sete Lagoas Formation. These successions define an overall shallowing upward pattern, marking a highstand systems tract (HST). An early highstand systems tract (EHST) is characterized by a thick mixed siliciclastic-carbonate facies deposited in the deeper carbonate ramp, grading upward into shallower mid-ramp microbial limestones. The late highstand systems tract (LHST) is marked by dark-gray pure microbial limestones mostly marking mid ramp strata that pass upward into high-energy shallow water carbonate facies. The late HST carbonate successions are associated with a remarkable basin-scale increase in the Sr/Ca on the carbonate deposits probably driven by enhanced alkalinity and/or aragonite precipitation (Caetano-Filho et al., 2019; Paula-Santos et al., 2020). The whole HST shows relatively stable $\delta^{13}C_{carb}$ values near 0‰ (e.g. Vieira et al., 2007; Kuchenbecker et al., 2016; Reis and Suss, 2016; Paula-Santos et al., 2017; Caetano-Filho et al., 2019).

A sequence boundary between the two 2nd-order sequences is marked by a major subaerial exposure recorded by supratidal carbonate deposits (Reis and Suss, 2016; Caetano-Filho et al., 2019). The overlying 2nd-order sequence begins with deposition of transgressive limestones of the upper Sete Lagoas Formation and deep water deposits from the Serra de Santa Helena Formation. These deposits grade upward into regressive deltaic-related and platformal siliciclastics of the middle to upper Serra de Santa Helena Formation and shallow marine carbonates of the Lagoa do Jacaré Formationa (Reis et al., 2016, Fig. 1B).

In this sequence stratigraphic framework, the MIBE corresponds to the large positive $\delta^{13}C_{carb}$ excursion starting in the end of the regressive stage of the basal sequence, with high values persisting through the overlying 2nd-order sequence (e.g. Santos et al., 2004; Paula-Santos et al., 2017; Uhlein et al., 2019). It is characterized by gradual positive excursion in the deeper domains of forebulge grabens and by a sharp discontinuity in paleohigh successions (Caetano-Filho et al., 2019). The MIBE is accompanied by low $^{87}Sr/^{86}Sr$ ratios (~0.7075–0.7077; Paula-Santos et al., 2017, Fig. 1), very unradiogenic compared with the expected values for the late Ediacaran (>0.7080; e.g. Halverson et al., 2010). These isotope anomalies have been interpreted as the result of the progressive restriction of the Bambuí foreland system during the Brasiliano/Pan-African cycle at the end of Neoproterozoic Era (e.g. Paula-Santos et al., 2017). The foreland-related nature of the Bambuí Group and its progressive restriction through time are supported by paleogeographic reconstructions (e.g. Tohver et al., 2006), the tectono-sedimentary filling pattern of the basin as constrained by seismic and drill core data (Reis and Alkmim, 2015; Reis and Suss, 2016; Reis et al., 2017), and by a drastic change in detrital provenance at the transition between the two basal sequences. It is evidenced by U–Pb ages in detrital zircon grains, which change from Mesoproterozoic and Tonian in the basal sequence to exclusively Ediacaran in the overlying one, interpreted as resulting from a rapid source-rock exhumation within neighboring orogenic belts (Paula-Santos et al., 2015).

Late Ediacaran metazoan fossils *Cloudina* sp. and *Corumbella werneri* (549−541 Ma; Grotzinger et al., 2000; Amthor et al., 2003) were reported in the middle Sete Lagoas Formation (~40–50 m from the basement; Warren et al., 2014; Perrella Jr. et al., 2017), ascribed to the LHST of the basal sequence (Caetano-Filho et al., 2019). U–Pb ages for detrital zircon grains provide a maximum depositional age of 560 Ma for the overlying sequence, in the upper Sete Lagoas Formation (Paula-Santos et al., 2015) (Fig. 1B). The cap carbonate interval at the base of the unit presents contrasting Pb–Pb isochron ages for different areas of the basin (740 ± 22 Ma, Babinski et al., 2007; 608 ± 19 Ma, Caxito et al., 2018). Pb–Pb isochron ages for the cap carbonate interval would imply a time span of at least ~80 m.yr.-long between the cap carbonate and the LHST of the basal 2nd-order sequence where *Cloudina* occurs. However, no stratigraphical evidence has been found so far to support the possible existence of condensation levels or hiatuses in the corresponding interval. Recent stratigraphic studies, based on detailed stratigraphic information from drill cores, indicate a continuous sedimentation in the basin throughout the basal sequences (Kuchenbecker et al., 2016; Reis and Suss, 2016; Caetano-Filho et al., 2019).

3. Materials and methods

3.1. Studied sections and previous $\delta^{13}C_{carb}$ and $\delta^{18}O_{carb}$ data

Here we report carbon isotope compositions of organic carbon for three stratigraphic sections. Two of them were sampled from continuous drill core that encompass the two basal 2nd-order sequences at the southern portion of the basin, along the Sete Lagoas basement high (Arcos and Well 1 sections; Figs. 1A, 2 and 3). The third one is a composite outcrop section sampled in the northern area, nearby Januária city (north of Minas Gerais state). It encompasses the two basal sequences on the Januária basement high (Januária section; Figs. 1A and 4). Detailed sedimentological description, $\delta^{13}C_{carb}$ and $\delta^{18}O_{carb}$ data for these sections were previously provided by Kuchenbecker et al. (2016), Reis and Suss (2016) and Caetano-Filho et al. (2019), and are summarized below. Stratigraphic correlation between the studied sections was carried with basis on the 2nd-order stacking patterns and bounding surfaces (e.g. Reis and Suss, 2016; Caetano-Filho et al., 2019 and references therein; Fig. 5). Two remarkable 2nd-order stratigraphic surfaces were identified: (i) the maximum flooding surface in the basal 2nd order sequence, and (ii) the sequence boundary between the two 2nd-order sequences, marked by unconformities and dolomitization processes that were described within basinal paleohighs (Arcos and Januaria sections). The HST was divided in early (EHST) and late (LHST) based on a basinal increase in Sr/Ca ratios. This increase is neither related to facies nor to carbonate content, and is recorded both in shallow- (Januária) and deep-water (Well 1) sections. It was interpreted as a significant paleoenvironmental change recorded throughout the basin, with possibly enhanced alkalinity, more aragonitic conditions and/or even hypersalinity, which persist to the overlying sequence (Figs. 2−4; Supplementary Table S1; Caetano-Filho et al., 2019; Paula-Santos et al., 2020).

3.1.1. Arcos section

The Arcos section is a 180 m-thick predominantly carbonate succession (Fig. 2). Transgressive strata are represented by a thin layer of polymictic diamictite of the Carrancas Formation unconformably overlying the Archean basement and intraclastic and mixed siliciclastic-carbonate grainstones and packstones of the Sete Lagoas Formation (Fig. 6A). These successions grade upward into calcimudstones with aragonite pseudomorph crystal fans (Fig. 6B), as typical features of cap

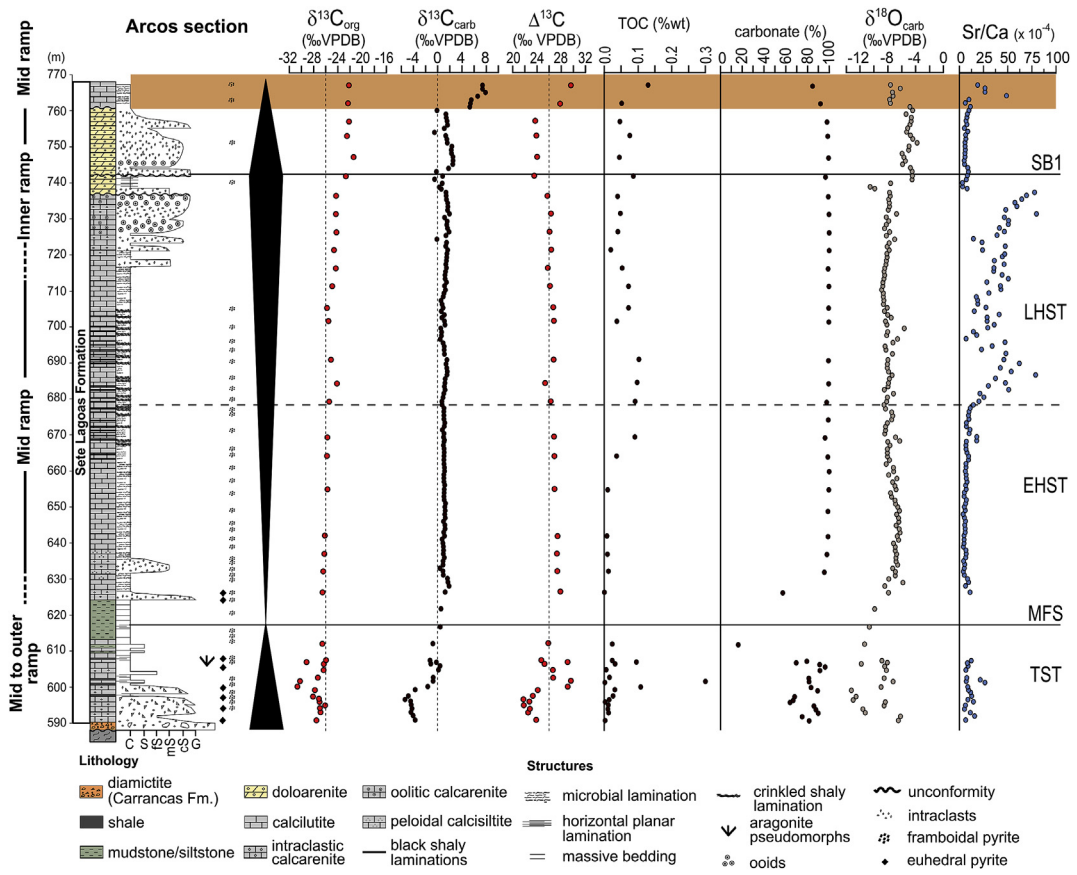

Fig. 2. $\delta^{13}C_{org}$, $\delta^{13}C_{carb}$ and $\Delta^{13}C$ evolution of the Arcos section. $\delta^{13}C_{carb}$, $\delta^{18}O_{carb}$ and Sr/Ca ratios from Kuchenbecker et al. (2016) and Caetano-Filho et al. (2019). Orange rectangle marks the MIBE interval.

carbonates. A massive layer of greenish siltstones sets the 2nd-order maximum flooding surface. The EHST stage encompasses pure microbial limestones (Fig. 6C), which persist through most part of the LHST. The upper part of LHST encompasses shallower facies represented by intraclastic to peloidal packstones/grainstones (Fig. 6D) and oolitic grainstones. Dolomitization processes affected these shallow water carbonate facies within the 2nd-order sequence boundary, which was set in a collapse breccia layer (Fig. 2; Kuchenbecker et al., 2016). This process was accompanied by dissolution, culminating with vugular and moldic porosity (Fig. 6E). In the overlying sequence, above the shallow water dolostone interval, dark-gray calcimudstones (Fig. 7A) and microbial limestones of the upper Sete Lagoas Formation mark a new transgressive systems tract (Fig. 2).

Regarding $\delta^{13}C_{carb}$ and $\delta^{18}O_{carb}$ data (Fig. 2; Supplementary Table S1; Kuchenbecker et al., 2016; Caetano-Filho et al., 2019), the TST encompasses a negative-to-positive excursions for both $\delta^{13}C_{carb}$ and $\delta^{18}O_{carb}$ profiles, typical of cap carbonate deposits. From the base of the section to the base of EHST, $\delta^{13}C_{carb}$ starts with values around −4‰ down to −5‰, followed by a positive excursion to 1‰, whereas $\delta^{18}O_{carb}$ initiates with values from −6‰ to −13‰, with a recover to values around –8‰ (Fig. 2). $\delta^{13}C_{carb}$ and $\delta^{18}O_{carb}$ profiles remain in a plateau through the whole HST, with values around 1‰ and −8‰, respectively. The dolostone interval presents $\delta^{13}C_{carb}$ values between 0 and 2‰, with some slightly negative spikes. $\delta^{18}O_{carb}$ values of dolostones are heavier compared with the rest of the section, reaching −4‰, which was interpreted as a possible influence of saline brines during early diagenetic dolomitization (Caetano-Filho et al., 2019). Above the dolostone interval, dark gray limestones from the upper sequence presents abrupt isotope shifts, as a positive $\delta^{13}C_{carb}$ excursion from 5‰ to 8‰, and $\delta^{18}O_{carb}$ in a plateau around −8‰ (Fig. 2).

3.1.2. Well 1 section

The Well 1 section is a 430 m-thick mixed siliciclastic-carbonate succession deposited in a forebulge graben domain, representing deeper environments and the thickest succession of the basal sequences of Bambuí Group (Fig. 3; Reis and Suss, 2016; Caetano-Filho et al., 2019). Within its basal transgressive systems tract, it contains a thin layer of polymictic diamictite of the Carrancas Formation, which grades upward into microbial dolostones (Fig. 6F) of the basal Sete Lagoas Formation (Fig. 3) and thick organic-rich black shales. These fine-grained siliciclastics define a 2nd-order maximum flooding surface (Figs. 3 and 6G). The early highstand systems tract (EHST) is marked by the overlying greenish siltstones interbedded with light gray limestones (Fig. 6H), which were deposited under the influence of storm waves and restricted subaqueous gravitational flows in outer to mid-carbonate ramp setting (Reis and Suss, 2016). These strata grade upward into mid-to inner-carbonate ramp successions composed of intraclastic grainstones to packstones, mudstones oolitic grainstones and microbial limestones (Fig. 7B). Fine to coarse-grained limestones comprise the late highstand systems tract (LHST), which is bounded in the top by a 2nd-order erosional surface recorded within supratidal carbonate deposits (Fig. 3; Reis and Suss, 2016). In the overlying 2nd-order sequence, dark gray microbial limestones of the upper Sete Lagoas Formation grade into fine-grained siliciclastics of the Serra de Santa Helena Formation, defining the new transgressive systems tract (Figs. 3 and 7C).

For the basal dolostone interval, the $\delta^{13}C_{carb}$ profile presents a slightly negative excursion from −3‰ to −4‰, coupled to a negative $\delta^{18}O_{carb}$ excursion from −7‰ to −10‰ (Fig. 3). Although these dolostones lack sedimentary features typical of cap carbonates, the gradual contact with the underlying diamictite from Carrancas Formation, the observed isotope excursions and available subsurface data allow correlate these

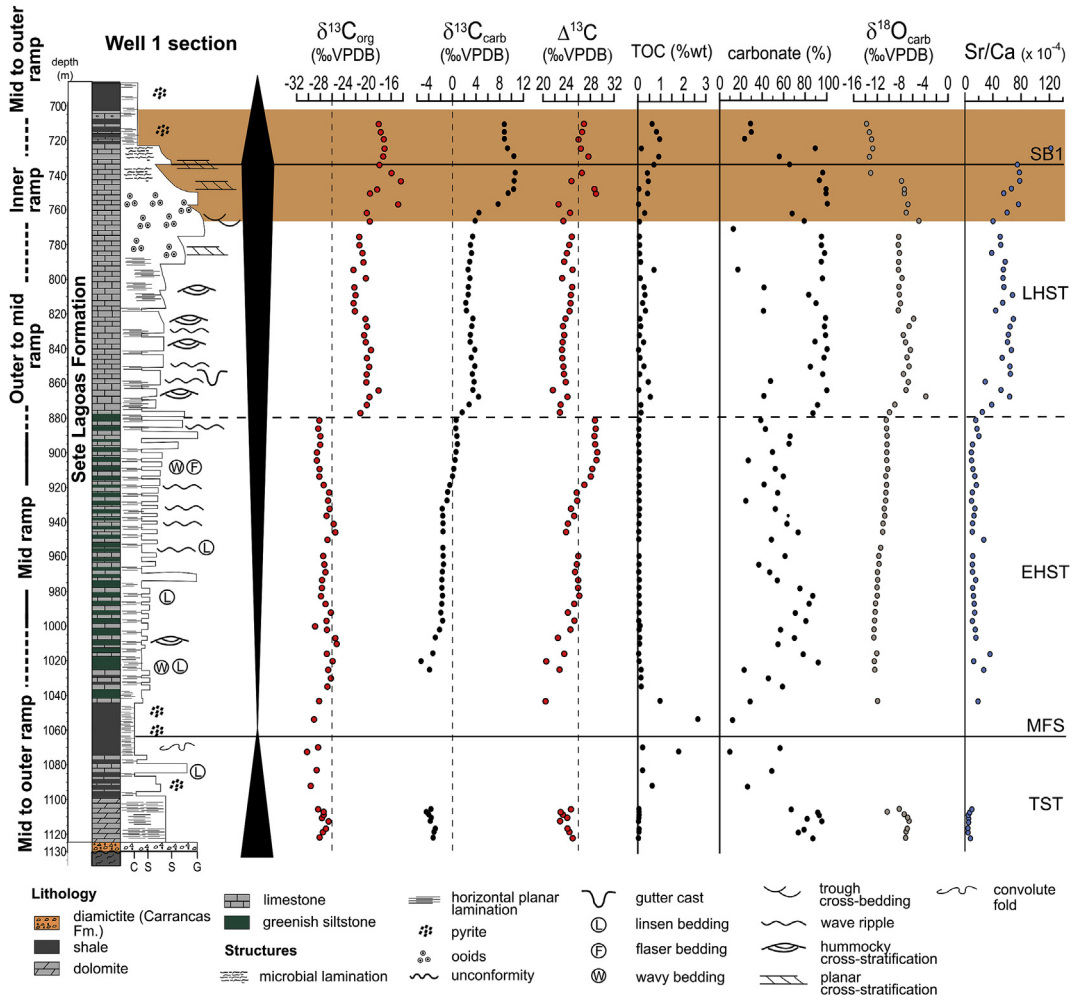

Fig. 3. $\delta^{13}C_{org}$, $\delta^{13}C_{carb}$ and $\Delta^{13}C$ evolution of the Well 1 section. $\delta^{13}C_{carb}$, $\delta^{18}O_{carb}$ and Sr/Ca ratios from Caetano-Filho et al. (2019). Orange rectangle marks the MIBE interval.

successions with other cap carbonate successions in the basin (Fig. 5). Above the thick transgressive black shale interval, the $\delta^{13}C_{carb}$ profile increases progressively from −7‰ to 0‰ within the EHST deposits (Fig. 3), accompanied by a $\delta^{18}O_{carb}$ increase from −12‰ to −10‰. The transition between EHST and LHST is marked by an increase in $\delta^{13}C_{carb}$ values to a plateau around 3‰. LHST exhibits $\delta^{18}O_{carb}$ values ranging between −6‰ and −8‰. The MIBE is set in the end of LHST, as an extreme $\delta^{13}C_{carb}$ positive excursion from 4‰ to 11‰, followed by a slight decrease to values near 9‰ in the overlying sequence (Fig. 3). The $\delta^{18}O_{carb}$ values drop to −13‰ during MIBE in Well 1 section.

3.1.3. *Januária section*

The Januária section is a ~140 m-thick carbonate-dominated succession that record some of the shallowest domains observed among the studied sections (Fig. 4). It contains within its basal portion the transgressive cap carbonate succession of the lower Sete Lagoas Formation, which unconformably overlies Archean/Paleoproterozoic basement assemblages. The cap carbonate is composed of massive layers of light gray calcimudstones and microbial limestones with common occurrences of aragonite pseudomorph crystal fans (Fig. 6I) and grades upward into reddish to pinkish calcimudstones to microbial limestones (Fig. 6J). Bounded by 2nd-order maximum flooding surface, this transgressive systems tract is overlain by highstand pinkish to light gray calcimudstones with hummocky cross-stratifications and abundant terrigenous clay laminae (Fig. 4; Caetano-Filho et al., 2019). The EHST and the lower portion of the LHST in the Januária section are dominated by dark gray microbial limestones (Fig. 6K), commonly comprising meter-scale cycles with storm-bedded grading upward to rippled limestones. The upper LHST, on the other hand, is dominated by flat pebble intraclastic carbonate breccias, interpreted as proximal deposits from gravitational flows developed in response to exposure and reworking of inner ramp strata (Perrella Jr. et al., 2017; Caetano-Filho et al., 2019), and peritidal carbonate successions. Sequence boundary was set at the base of an overlying dolostone interval, represented by intertidal facies with sigmoidal cross-stratification (Fig. 6L), at the top of Sete Lagoas Formation. The transgressive systems tract of the overlying 2nd-order sequence is recorded mostly by siltstones from the Serra de Santa Helena Formation. These strata grade upward into regressive shallow water carbonate facies of the Lagoa do Jacaré Formation, which are made up by laminated calcimudstones (Fig. 7D), intraclastic grainstones (Fig. 7E) and subordinated layers of carbonate breccias.

The $\delta^{13}C_{carb}$ profile starts with typical negative-to-positive excursion associated with cap carbonate interval, from −3‰ to −5‰, followed by a recover to values between −1‰ and 0‰ (Fig. 4). $\delta^{18}O_{carb}$ covaries with $\delta^{13}C_{carb}$, in a negative excursion from −14‰ to −16‰, followed by a positive excursion to −9‰. After the maximum flooding surface, the $\delta^{13}C_{carb}$ profile presents a plateau of values between 0 and 1‰ for the whole HST stage. The $\delta^{18}O_{carb}$ profile also presents a plateau of values around −6‰, with a slight decrease to −9‰ at the end of LHST stage. In the overlying sequence, shallow water carbonate facies from the Lagoa do Jacaré Formation represents the MIBE in Januária section, with extreme $\delta^{13}C_{carb}$ values near 12‰, reaching up to 14‰. $\delta^{18}O_{carb}$ profile

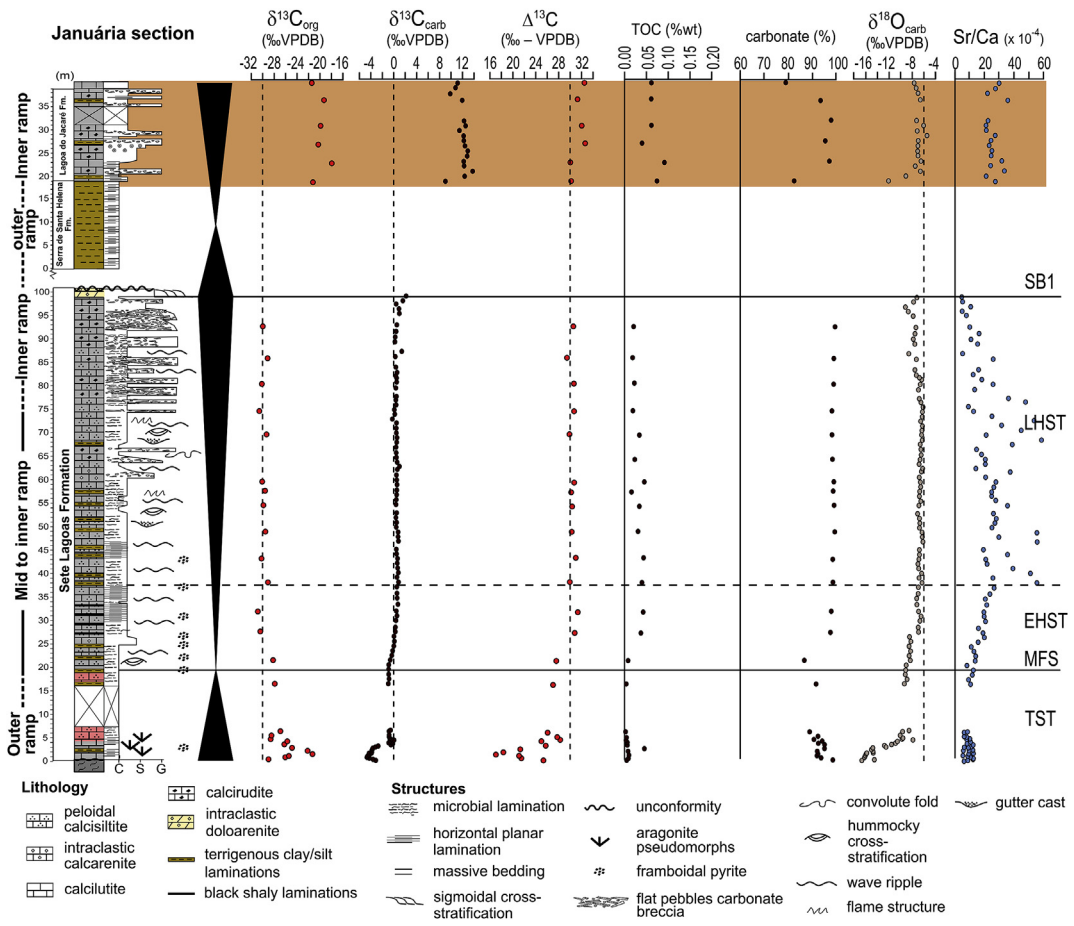

Fig. 4. $\delta^{13}C_{org}$, $\delta^{13}C_{carb}$ and $\Delta^{13}C$ evolution of the Januária section. $\delta^{13}C_{carb}$, $\delta^{18}O_{carb}$ and Sr/Ca ratios from Caetano-Filho et al. (2019). Orange rectangle marks the MIBE interval.

are relatively stable near −7‰ during this interval (Fig. 4).

3.2. Carbonate and TOC contents and $\delta^{13}C_{org}$ analyses

A subset of 158 samples previously analyzed for $\delta^{13}C_{carb}$ (Caetano-Filho et al., 2019) was selected for $\delta^{13}C_{org}$ analyses, in a stratigraphic resolution of 1 m for the cap carbonate interval (except Well 1 section, with 3 m resolution) and 5 m for the rest of section. Organic carbon was analyzed after a pre-acidification to remove the carbonate phases. About 3–5 g of carbonate rock powder were reacted with 25 mL of HCl 5 N 12 h at 25 °C then heated at 80 °C for 2 h. Residues were rinsed three to four times in distilled water until reaching neutral pH then dried in an oven at 50–60 °C. Insoluble residues were weighted allowing the carbonate contents to be calculated (Supplementary Table S1). About 5–10 mg of the decarbonated powder were weighted in tin capsules for measurements of TOC and $\delta^{13}C_{org}$ in an elemental analyzer Thermo Scientific EA Flash 2000 coupled to a Thermo Scientific Delta V+ at the Pôle de Spectométrie Océan, University of Western Brittany, France. The detailed mass spectrometry methodology is described in Pasquier et al. (2018). A total of 158 organic carbon stable isotope compositions were measured. $\delta^{13}C_{org}$ average uncertainty calculated based on measurements of internal standard was lower than 0.2‰ (2σ).

4. Results

4.1. Carbonate and TOC content

Isotope data, TOC and carbonate content are given in Supplementary Table S1. Carbonate facies dominates the base of Bambuí Group, with limestone samples yielding average and median carbonate contents of 81% and 91%, respectively. Black shale intervals from the Well 1 section (Fig. 3) present average and median carbonate contents of 31% and 28%, respectively. Overall, TOC values are low, varying from 0.00 to 2.64%. TOC values higher than 0.50% are only reported for black shale intervals in Well 1 section. The rest of the section exhibits an average TOC content of 0.12% (n = 76), with the EHST siliciclastic interval exhibiting the lowest values (Fig. 3). Januária and Arcos sections yield very low TOC contents, with an average value of 0.04% (n = 75; Figs. 2 and 4).

4.2. $\delta^{13}C_{org}$, $\delta^{13}C_{carb}$ and $\Delta^{13}C$ patterns

$\delta^{13}C_{org}$ data for the three studied sections is shown in Figs. 2–5 together with $\delta^{13}C_{carb}$ previously obtained for the limestone samples (Caetano-Filho et al., 2019) and the isotope difference between carbonate and organic matter ($\Delta^{13}C = \delta^{13}C_{carb} - \delta^{13}C_{org}$). Our data reveal that $\delta^{13}C_{org}$ and $\delta^{13}C_{carb}$ trends are independent of sedimentary facies, and record similar trends trackable at a basinal scale, from shallow to deep parts of the carbonate ramp, with exception of terrigenous-rich EHST interval from Well 1 section (Fig. 5). Three main isotope patterns are observed, which coincide with previously identified chemostratigraphic intervals (CI-1, CI-2 and CI-3) and sequence stratigraphic stages (Paula-Santos et al., 2017; Caetano-Filho et al., 2019):

(i) In the cap carbonate interval at the base of Sete Lagoas Formation, corresponding to part of the TST of the first sequence, $\delta^{13}C_{carb}$ starts at around −5‰ and increases upward to values of 0‰ (CI-1; Fig. 5). The $\delta^{13}C_{org}$ is decoupled from the $\delta^{13}C_{carb}$, with an antithetical behavior, starting with a $\delta^{13}C_{org}$ increase from about

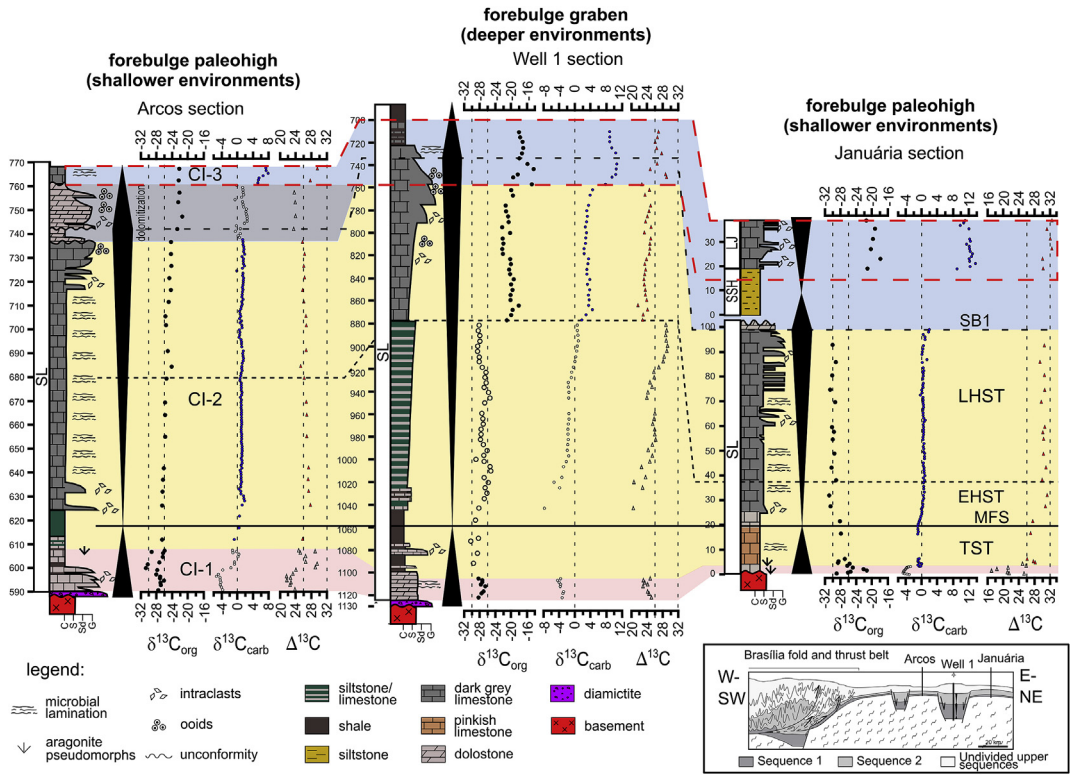

Fig. 5. $\delta^{13}C_{org}$, $\delta^{13}C_{carb}$ and $\Delta^{13}C$ evolution for the three studied sections representing basal Bambuí Group. Correlation lines represent sequence stratigraphy division from Caetano-Filho et al. (2019): TST – Transgressive Systems Tract; EHST – Early Highstand Systems Tract; LHST – Late Highstand Systems Tract; MFS – Maximum Flooding Surface; SB1 – Sequence Boundary 1. Lithostratigraphy: SL – Sete Lagoas Formation; SSH – Serra de Santa Helena Formation; LJ – Lagoa do Jacaré Formation. Colored intervals represent Chemostratigraphic Intervals (CI) from Paula-Santos et al. (2017). Granulometry scale: C – clay; S – silt; Sd – sand; G – gravel. Open symbols mark samples that were interpreted as possible altered. The red dashed rectangle highlights the MIBE interval. In the bottom right corner, the schematic seismic profile for São Francisco basin with the position of sections in the forebulge domain (modified from Reis and Suss, 2016).

−29‰ to about −25‰, in Arcos and Well sections (Figs. 2 and 3, respectively), and to the highest value of ~ −21‰ in Januária section, followed by a decline to values of about −30‰ (Fig. 4). Consequently, the $\Delta^{13}C$ profile evolves dramatically, attaining values lower than 25‰ when $\delta^{13}C_{carb}$ values are negative.

(ii) At the middle of the Sete Lagoas Formation, at the end of the TST and throughout the HST, $\delta^{13}C_{carb}$ values form plateaus around 0‰, except for Well 1 section (CI-2; Fig. 5). $\delta^{13}C_{org}$ profiles also form plateaus at values around −30‰ in Januária and −25‰ in Arcos. Consequently, lateral variations are also observed in $\Delta^{13}C$ values, from +30‰ in Januária to +26‰ in Arcos. Well 1 section shows a distinct pattern for this interval. $\delta^{13}C_{carb}$ varies from around −2‰ in the EHST, to +4‰ in the LHST, while $\delta^{13}C_{org}$ increases from −27‰ to −21‰. There is a marked discontinuity for both $\delta^{13}C_{carb}$ (from 0 to +4‰) and $\delta^{13}C_{org}$ (from –28‰ to –20‰), clearly controlled by a lithological change from high-frequency interbedded siltstones and limestones to very pure dark-colored limestone, which results in a sharp $\Delta^{13}C$ decrease from +29‰ to +24‰.

(iii) Right below the sequence boundary in Well 1 section or slightly above it in the two other sections, heavy isotope compositions are observed for both $\delta^{13}C_{carb}$ and $\delta^{13}C_{org}$ (CI-3; Fig. 2). $\delta^{13}C_{carb}$ values reach +14‰ (Januária section) whereas $\delta^{13}C_{org}$ values can reach –14‰ (Well 1 section). Minor differences in $\delta^{13}C_{carb}$ and $\delta^{13}C_{org}$ values between sections result in slight differences in $\Delta^{13}C$ values, which are around +31‰ in Januária section, +28‰ in Arcos section and +27‰ in Well 1 section. The transition between the chemostratigraphic intervals 2 and 3 (CI-2 to CI-3) is not recorded in Januária section, whereas in Arcos section it is represented by a dolostone interval.

5. Discussion

5.1. Assessing putative $\delta^{13}C_{carb}$ and $\delta^{13}C_{org}$ diagenetic overprints and the significance of $\Delta^{13}C$

$\Delta^{13}C$ values potentially record information on the type of photosynthesis (e.g. oxygenic *vs* anoxygenic photosynthesis) or on its conditions of operation (e.g. high *vs* low $[CO_2]_{aq}$; Hayes et al., 1999). But before such values are interpreted in these terms it is essential to verify that organic matter and carbonates were formed from the same DIC pool. Specifically, this implies that organic and carbonate carbon isotope compositions have not been overprinted by post-depositional processes, and that neither carbonate nor organic matter are detrital, remobilized from another depositional environment or formed in separate zones of the water column presenting contrasted DIC isotope signatures.

Experimental studies and observations on modern environments show that post-depositional processes impacting the isotope values of the organic carbon fraction, such as early diagenetic microbial activity, thermal maturation, and metamorphism result in a maximum of about ±2‰ difference in the $\delta^{13}C_{org}$ (e.g. McKirdy and Powell, 1974; Macko et al., 1994; Lehmann et al., 2002; Galimov, 2004; Simoneit et al., 2004; Yamaguchi et al., 2010). In our samples, the limited influence of oxidative weathering of sedimentary organic matter is confirmed by the good agreement of $\delta^{13}C_{org}$ chemostratigraphic evolution between sections sampled from drill cores (Arcos and Well 1; Figs. 2, 3 and 5) and the section sampled from outcrops (Januária; Figs. 4 and 5), and with their respective stratigraphic evolution. Considering that drill core sampling from Arcos and Well 1 sections come from different parts of the basin (forebulge paleohigh and forebulge graben) most likely representing distinct burial conditions, the coupled stratigraphic-chemostratigraphic

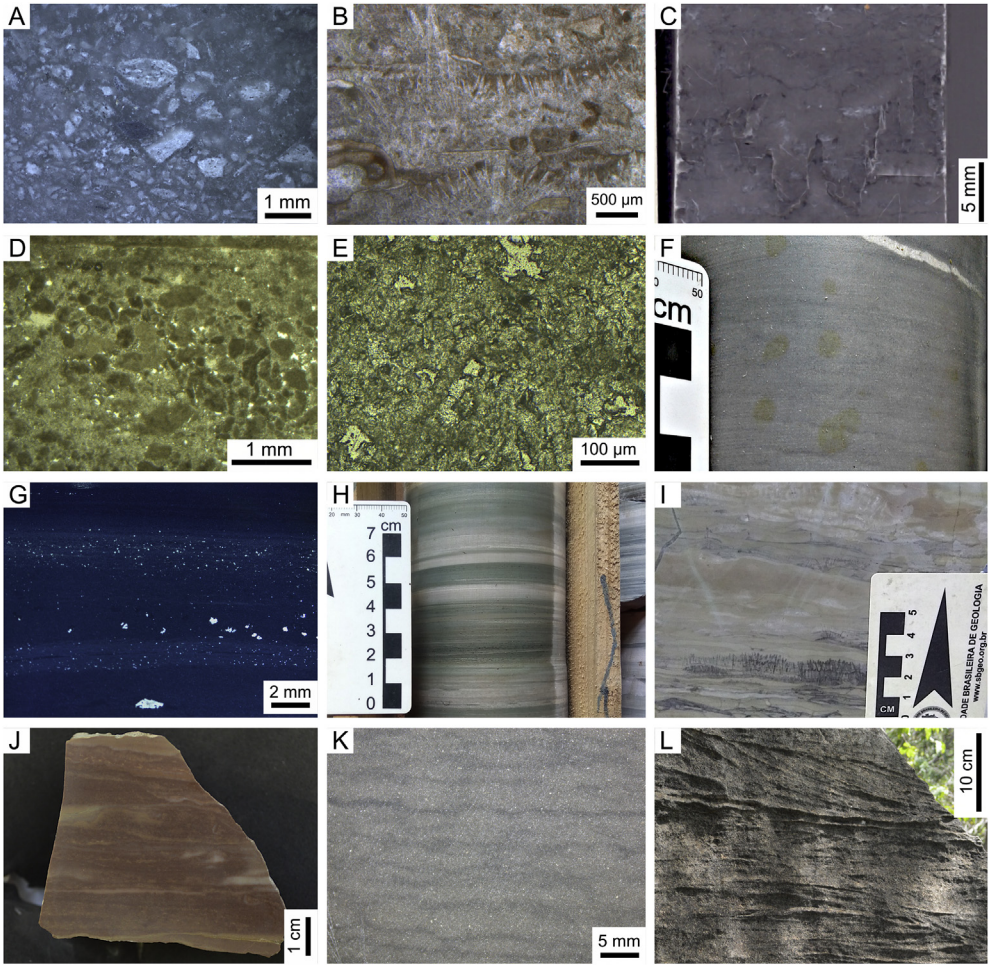

Fig. 6. Sedimentary facies from the basal Sete Lagoas Formation, representing the basal sequence from the Bambuí Group. (A) Intraclastic grainstone from cap carbonate interval of Arcos section. This basal interval presents frequent filled fractures and fluid percolation features. (B) Plane polarized thin section image of calcimudstone from the cap carbonate interval of the Arcos section. Detail for aragonite pseudomorph crystal fans. (C) Polished slab of a microbial limestone from the HST stage of the Arcos section. (D) Plane polarized thin section image of peloidal packstone from the LHST stage of the Arcos section. (E) Plane polarized thin section image from dolostone from the top of Arcos sections, showing intense dolomitization and vugular porosity. (F) Microbial dolostone from cap carbonate interval of Well 1 section. (G) Polished slab from a black shale sample from the base of Well 1 section. (H) High frequency greenish siltstones and gray calcimudstones interbedding from the EHST stage of the Well 1 section. (I) Calcimudstone with aragonite pseudomorph crystal fans from the cap carbonate interval from Januária section. (J) Polished slab of a reddish calcimudstone from the TST stage of Januária section. (K) Polished slab of a microbial limestone from the HST stage of the Januária section. (L) Outcrop of the dolostone interval from the upper part of basal sequence in Januária section, with tangential cross-stratification.

trends also argue against the influence of oxidative weathering during the post-depositional evolution of the studied strata. In addition, the lack of correlation between TOC and $\delta^{13}C_{org}$ (Fig. 8A–C) also supports the idea that early diagenetic alteration of organic matter does not seem to control, at least to the first order, the observed $\delta^{13}C_{org}$ variations in the studied sections. Regardless the thermal maturity of the studied samples (Reis and Suss, 2016), no metamorphic features have been observed suggesting a limited influence of thermal processes on their overall carbon isotopic content. Hence, the full range of $\delta^{13}C_{org}$ values (from −32‰ to −17‰) observed in the studied sections cannot be accounted for post-depositional processes, even if minor influences of the order of 2‰ are possible.

In addition to the post-depositional alteration of the $\delta^{13}C_{org}$, another factor that can affect the $\Delta^{13}C$ is the presence of detrital organic matter. Here, the similarity of $\delta^{13}C_{org}$ trends at the basin scale argues against a detrital organic matter influence, considering that the sections are positioned hundreds of kilometers apart. It is unlikely that a detrital influence would dominate homogeneously the basinal $\delta^{13}C_{org}$ signal, specially resulting in uniformly high $\delta^{13}C_{org}$ values for the MIBE. Moreover, detrital lean limestones dominate the MIBE intervals in the studied sections (Figs. 2–4; Supplementary Table S1), supporting that a significant influence of detrital organic matter over the major isotope trends is unlikely. The EHST stage of Well 1 is an exception due to the dominance of siltstones and mudstones with very low TOC content (Fig. 3), and is the most susceptible interval for detrital organic contamination. The high amount of detrital material and low TOC content of this interval in Well 1 section (Fig. 3; Supplementary Table S1) may explain the facies-dependency behavior of $\delta^{13}C_{org}$ profile, which displays an abrupt increase at the transition with the overlying carbonate-dominated LHST interval.

In comparison, carbonate carbon isotope fractionation is more likely to be affected by post-depositional processes. As discussed in Caetano-Filho et al. (2019), the negative $\delta^{13}C_{carb}$ excursions recorded in the cap carbonates at the base of the studied sections and the positive $\delta^{13}C_{carb}$ excursion at the top (MIBE) are trackable at basinal scale and are not facies-dependent. This stratigraphic $\delta^{13}C_{carb}$ pattern was thus assumed to be primary at the 2nd-order. Here we can reevaluate this assumption using $\Delta^{13}C$ values, considering that $\Delta^{13}C$ values in the 26‰–32‰ range (Fig. 5) result from a typical photosynthesis isotope effect when CO_2 partial pressure is higher than 500 ppm, while lower value may potentially indicate altered $\delta^{13}C_{carb}$ values or distinct pools of DIC used for organic and carbonate reservoirs (e.g. Hayes et al., 1999). The majority of samples present $\Delta^{13}C$ values in the normal range, supporting the assumption that the isotope patterns are primary. Only a limited number of intervals present $\Delta^{13}C$ values lower than the 26‰–32‰ range, and require a reassessment of potential overprinting of $\delta^{13}C_{carb}$ values by diagenesis. These intervals are highlighted as empty symbols in Figs. 5 and 9 and correspond to: (i) the base of the cap carbonate interval in all sections; (ii) the major part of the early highstand stage at Well 1 section (from 1060 to 880 m depth); (iii) the major part of the late highstand stage at Well 1 section, and (iv) the dolostone interval in Arcos section.

Our analysis of the impact of diagenesis on $\delta^{13}C_{carb}$ will take in account petrological observations and covariation between $\delta^{18}O_{carb}$ and $\delta^{13}C_{carb}$. In addition, a negative trend in a TOC *vs* $\delta^{13}C_{carb}$ diagram (Fig. 8) can also be used to infer precipitation of early diagenetic carbonates, as a result of what is often called organic diagenesis, where microbial respiration of organic matter delivers ^{12}C-enriched carbon into the pore fluid (e.g. Ader and Javoy, 1998; Sansjofre et al., 2011). Such

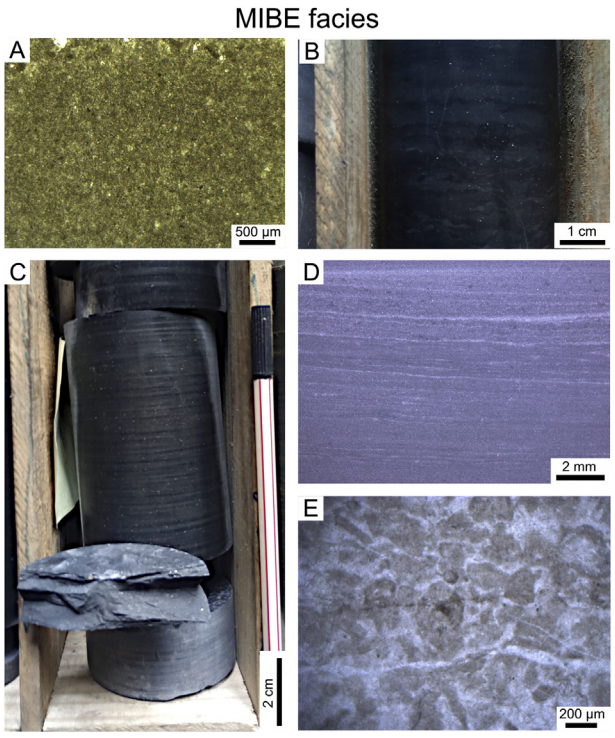

Fig. 7. Sedimentary facies from the MIBE interval. (A) Plane polarized thin section image of a calcimudstones from the Arcos section (Sete Lagoas Formation). (B) Drill core interval of microbial limestones from the Well 1 section (Sete Lagoas Formation). (C) High frequency interbedding of black shales and dark calcimudstones from the upper sequence of Well 1 section (Sete Lagoas Formation). (D) Polished slab of a laminated calcimudstone from the upper sequence of Januária section (Lagoa do Jacaré Formation). (E) Plane polarized thin section image of an intraclastic grainstone from the upper sequence of Januária section (Lagoa do Jacaré Formation).

trends are more likely to be seen in shaly intervals, where the low permeability prevents pore waters from equilibrating with the overlying seawater and the organic substrate is usually high for microbial respiration. The same trend could also result from organic carbon remineralization in late diagenesis processes, although it is less important due to low fluid/rock interactions in a highly compacted condition. In our samples, no correlation between TOC and $\delta^{13}C_{carb}$ (Fig. 8D–F) can be seen for intervals with low $\Delta^{13}C$, even when shaly levels are present. Therefore, it is not possible to conclusively argue that $\delta^{13}C_{carb}$ were overprinted by organic diagenesis.

Petrological observations allowed the recognition of features typical of carbonate diagenesis, such as dissolution and secondary crystallization, or the presence of levels more susceptible to post-depositional fluid percolation, such as abrupt lithological contacts (e.g. siliciclastic *vs* carbonate facies). Cap carbonates are affected by dolomitization in Well 1 section, by intense recrystallization in Januária section, with spatic white carbonate layer immediately above the contact with basement, filled-fractures and fluid percolation features (Fig. 6I), while in Arcos section they exhibit frequent interbedding of siltstones and shales at the base (Fig. 2). The dolostone interval at the top of Arcos section also displays intense recrystallization, followed by a dissolution event, which resulted in vugular porosity (Fig. 6E; Kuchenbecker et al., 2016; Caetano-Filho et al., 2019). In Well 1 section, the EHST is composed of high frequency interbedding of green siltstones/mudstones and limestones (Fig. 6H) that are lithological contacts favorable to fluid percolation. Finally, the LHST stage of Well 1 unlike the other intervals discussed before does not present petrological evidence of pervasive post-depositional fluid percolation, being composed of carbonate rocks with well-preserved textures (e.g. Fig. 7B; Reis and Suss, 2016; Caetano-Filho et al., 2019) and almost completely free of a detrital component (Fig. 3; Supplementary Table S1).

Covariations between $\delta^{18}O_{carb}$ and $\delta^{13}C_{carb}$ have been widely used to track diagenetic overprint on both $\delta^{18}O_{carb}$ and $\delta^{13}C_{carb}$ (e.g. Jacobsen and Kaufman, 1999). In a $\delta^{18}O_{carb}$ *vs* $\delta^{13}C_{carb}$ diagram no overall covariation can be seen for individual sections (Fig. 9A). Yet, if we consider only the samples with $\Delta^{13}C$ below 25‰, some intervals present positive trends (Fig. 9B). The cap carbonate intervals of all sections show a weak decrease of $\delta^{13}C_{carb}$ with $\delta^{18}O_{carb}$ following different trends. Notwithstanding, they present similar $\delta^{13}C_{carb}$ values for contrasting $\delta^{18}O_{carb}$ in each section, which suggests diagenetic alteration of $\delta^{13}C_{carb}$ was minor in these rocks, at least during diagenetic events responsible for the $\delta^{18}O_{carb}$ variability. The EHST and LHST of Well 1 both show positive $\delta^{13}C_{carb}$ and $\delta^{18}O_{carb}$ trends, with steep and gentle slopes, respectively (Fig. 9B). The diagenetic control of $\Delta^{13}C$ on these two segments of the Well 1 section can be further inspected with the $\Delta^{13}C$ *vs* $\delta^{13}C_{carb}$ diagram

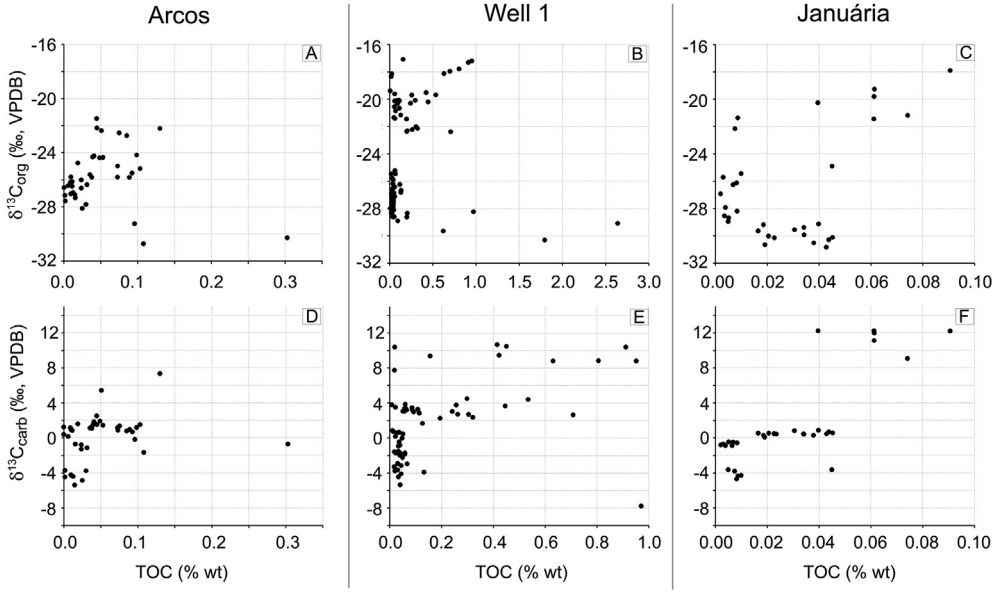

Fig. 8. TOC *vs* $\delta^{13}C_{carb}$ and TOC *vs* $\delta^{13}C_{org}$ diagrams for the three studied sections.

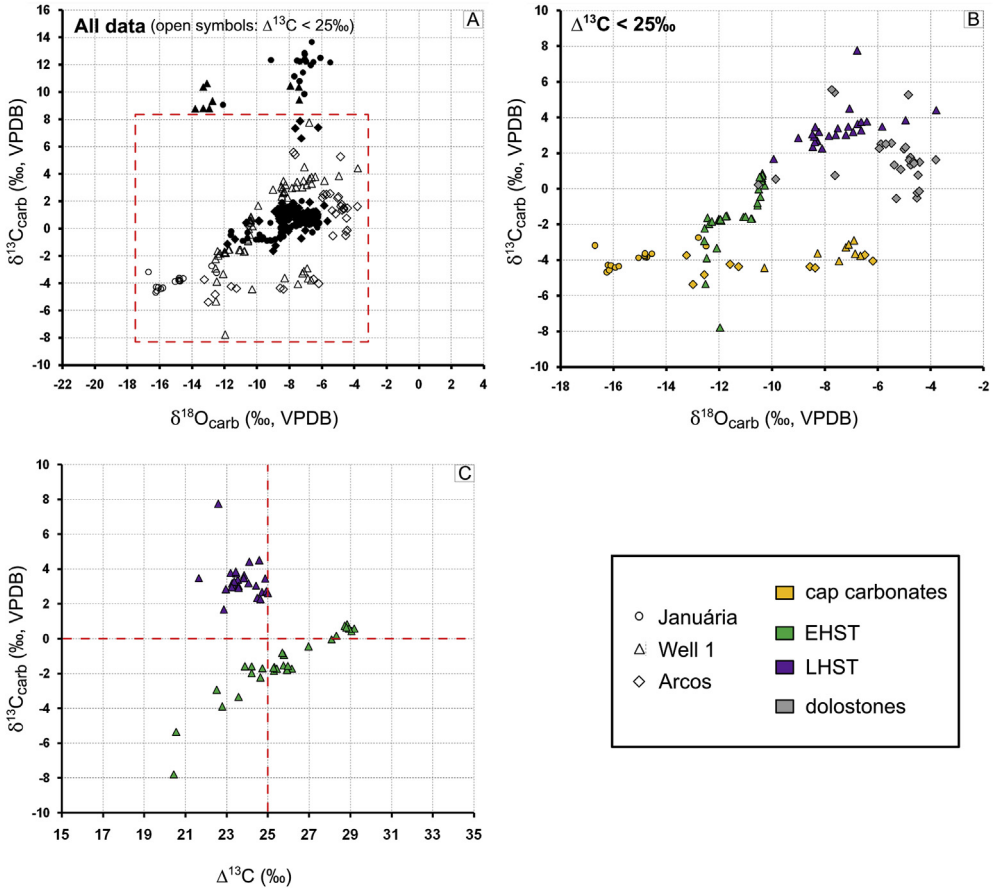

Fig. 9. (A) $\delta^{18}O_{carb}$ *vs* $\delta^{13}C_{carb}$ diagram for all the data. Open symbols represent those data with unusual $\Delta^{13}C < 25‰$, whereas the filled points represent $\Delta^{13}C > 25‰$. (B) $\delta^{18}O_{carb}$ *vs* $\delta^{13}C_{carb}$ diagram with only data with $\Delta^{13}C < 25‰$ (dashed rectangle in diagram A), distinguished per section and stratigraphic stage. (C) $\Delta^{13}C$ *vs* $\delta^{13}C_{carb}$ diagram for EHST and LHST stage of the Well 1 section, note that negative $\delta^{13}C_{carb}$ values of the EHST stage is associated with $\Delta^{13}C < 25‰$.

(Fig. 9C). A clear 1:1 slope is observed for EHST intimately associating $\Delta^{13}C$ below 25‰ to negative $\delta^{13}C_{carb}$ values, which strongly suggests a diagenetic overprint of the carbonate carbon isotope compositions of this specific interval. In contrast, no correlation is observed for LHST. Therefore samples from LHST were further considered in our paleoenvironmental analysis, whereas those from the EHST were discarded. Finally, the dolostone interval in Arcos section does not present a $\delta^{13}C_{carb}$ and $\delta^{18}O_{carb}$ positive covariation, but it displays the most positive $\delta^{18}O_{carb}$ values of all samples, suggesting an early diagenetic dolomitization related to saline brines (Caetano-Filho et al., 2019). Furthermore, occurrences of dissolution features associated with dolomitization in this interval (Fig. 6E) lead to a conservative assumption to avoid paleodepositional interpretations over the carbon isotope signatures of these rocks.

In sum, considering that their $\delta^{13}C_{carb}$ values are likely to have been overprinted during diagenesis none of the intervals with anomalously low $\Delta^{13}C$ were considered for further paleoenvironmental interpretation except for the LHST in Well 1 section. Nevertheless, omitting these intervals do not compromise the discussion concerning the MIBE, in which extreme positive $\delta^{13}C$ excursions (>10‰) occur, without significant changes in $\Delta^{13}C$ (<3‰ in magnitude; Fig. 5). In addition, although paired carbon isotope signatures from the cap carbonate interval are considered potentially altered in our sample screening, low $\Delta^{13}C$ values are typically described in other Ediacaran cap carbonate successions (e.g. Sansjofre et al., 2011). For this reason, the cap carbonate interval is discussed in a separate section before discussing the MIBE, considering they represent remarkable carbonate deposits in geological record and data presented here can be of interest for future studies on this topic.

5.2. *Non facies-dependent and antithetical $\delta^{13}C_{carb} - \delta^{13}C_{org}$ trends for the basal Sete Lagoas Formation: a typical cap carbonate $\Delta^{13}C$ excursion?*

Low $\Delta^{13}C$ values are usually reported for Ediacaran cap carbonates (~19‰–24‰; Sansjofre et al., 2011 and references therein; and as low as 17‰ by this study; Januária section – Fig. 4), compared with the interglacial periods of late Neoproterozoic (28‰–32‰; Hayes et al., 1999). This results from decoupling and apparent inverse relationship between $\delta^{13}C_{carb}$ and $\delta^{13}C_{org}$ (e.g. Jiang et al., 2010; Sansjofre et al., 2011, Figs. 2–5). Changes in the photosynthetic fractionation factor (ε_p) (e.g. Hayes et al., 1999; Sansjofre et al., 2011), active uptake of HCO_3^- during photosynthesis (Jiang et al., 2010), diagenesis and allochthonous input of organic carbon (Jiang et al., 2012) were hypotheses proposed to explain such anomalously low values of $\Delta^{13}C$ in cap carbonate successions.

We report here that the new paired $\delta^{13}C$ data from Bambuí Group cap carbonates, from shallow to deep domains of the carbonate ramp (Fig. 5), show that major carbon isotope trends are not facies-dependent. These trends are equally recorded in intraclastic grainstones (Fig. 6A), rudstones and calcilutites in Arcos section, microbial limestones and calcimudstones bearing aragonite pseudomorph crystal fans in Arcos and Januária sections (Fig. 6B and I, respectively), and microbial dolostones followed by distal black shales in Well 1 section (Figs. 3 and 6F) (Caetano-Filho et al., 2019). Thus, detrital organic matter influence can be discarded in our case, especially considering the dominantly pure carbonate facies usually associated with this interval (Supplementary Table S1). Given the clear stratigraphic control over these excursions and the fact that the different sections likely experienced different burial rates (graben and paleohighs), late diagenesis is also not likely. Therefore, a

primary or very early diagenetic origin for the mirrored $\delta^{13}C_{carb} - \delta^{13}C_{org}$ trends observed here remains possible (e.g. Knauth and Kennedy, 2009; Jiang et al., 2010; Sansjofre et al., 2011).

5.3. Extreme positive $\delta^{13}C$ excursion in the late Ediacaran-Cambrian Bambuí Group: a methanogenic-dominated basin?

When omitting the samples possibly affected by post-depositional perturbations, our paired $\delta^{13}C$ data show that the extreme positive $\delta^{13}C_{carb}$ excursion (MIBE) is nicely coupled to the $\delta^{13}C_{org}$ with a very strong positive correlation for all the studied sections (correlation coefficients of 0.90, 0.83 and 0.99 for Arcos, Well 1 and Januária sections, respectively, $p(\alpha) < 0.01$; Fig. 10). The $\Delta^{13}C$ patterns of each section show a maximum increase of 3‰ in the MIBE (Well 1 section) compared with the underlying intervals, in spite of a 10‰ $\delta^{13}C_{carb}$ isotope excursion (Fig. 5). Together with a range of $\Delta^{13}C$ values compatible with carbonates and organic matter acquiring their isotope value from the same DIC reservoir (Hayes et al., 1999), this suggests that the MIBE was driven by extreme increase in the $\delta^{13}C_{DIC}$ value of seawater through the whole basin, from shallow to deeper environments.

The MIBE seems to have been strongly controlled by the tectonic evolution of the basin, as indicated by its relationship with the basal 2nd-order sequence boundary in the Bambuí foreland system. This basal sequence boundary is accompanied by a drastic change in provenance data with relatively young zircon grains in the second sequence, indicating the advance of the mountain belts surrounding the São Francisco Craton during late Ediacaran-Cambrian (Paula-Santos et al., 2015; Reis et al., 2016). Geochemical inferences for a progressively restricted and isolated basin come from a basin-scale increase in Sr/Ca ratios preceding the MIBE, interpreted as a more alkaline, aragonitic, and/or hypersalinity conditions (Caetano-Filho et al., 2019), and from a drop in the $^{87}Sr/^{86}Sr$ ratios to 0.7075–0.7077, mismatching late Ediacaran-Cambrian global values (Paula-Santos et al., 2017). All of these arguments strongly suggest that the carbon cycle in the basin was also affected by the basin isolation in Gondwana interior and, therefore, the MIBE is here considered a local signal decoupled from the global carbon budget. This assumption is also supported by the fact that the MIBE presents values significantly higher than other upper Ediacaran–lower Cambrian successions, usually below 6‰ (e.g. Zhou and Xiao, 2007; Fike and Grotzinger, 2008; Halverson et al., 2010 and references therein), even considering other West Gondwana domains (Corumbá Group – $\delta^{13}C_{carb} < 5$‰, Boggiani et al., 2010; Arroyo del Soldado Group – $\delta^{13}C_{carb} < 4$‰; Gaucher et al., 2003). Similar heavy $\delta^{13}C_{carb}$ values (>10‰) are reported from coeval carbonate successions of São Francisco-Congo craton for carbonate units within orogenic belts surrounding Bambuí Group (Uhlein et al., 2019 and references therein), and from the Hüttenberg Formation, Otavi Group (Cui et al., 2018), which are assigned to the same restricted geotectonic scenario of West Gondwana assembly.

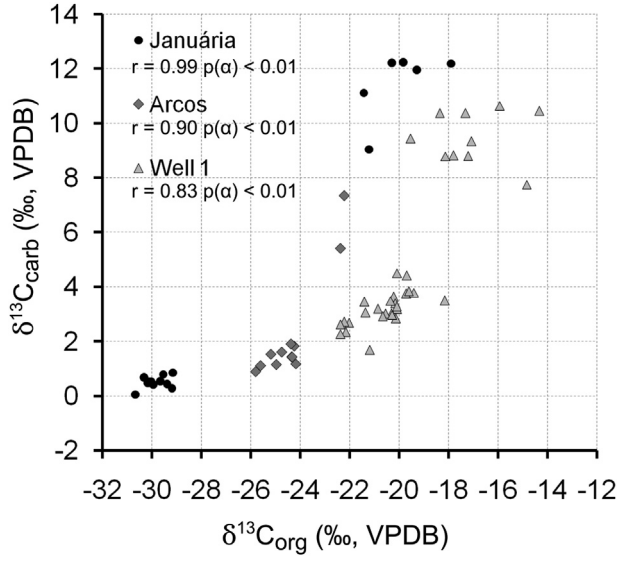

Fig. 10. $\delta^{13}C_{org}$ *vs* $\delta^{13}C_{carb}$ diagram for data through LHST and overlying sequence. The MIBE presents very strong correlation coefficient for all the studied sections, attesting that these isotope excursions represent the same DIC reservoir.

As previously discussed by Paula-Santos et al. (2017) and Uhlein et al. (2019), this positive $\delta^{13}C$ excursion would require unrealistic scenarios under steady-state mass balance assumptions, where the ocean and atmosphere are in isotope equilibrium ($\delta^{13}C_{input} = (1-f_{org}) \times \delta^{13}C_{carb} + f_{org} \times \delta^{13}C_{org}$; e.g. Hayes et al., 1999). The coupled carbon excursions presented here, reaching up to +14‰ and −14‰ for $\delta^{13}C_{carb}$ and $\delta^{13}C_{org}$ respectively, would require a fraction of organic carbon buried (f_{org}) higher than 50% or increased $\delta^{13}C_{input}$ above +4‰, more than 9‰ above the bulk value of −5‰. On the other hand, the MIBE might not fit time-dependent non-steady state scenarios, in which a decreased DIC reservoir leads to higher sensitivity of the marine carbon isotope system (i.e. extreme isotope excursions would not require dramatic changes in f_{org} and $\delta^{13}C_{input}$, e.g. Bartley and Kah, 2004). Carbonate rocks from the Bambuí Group towards the MIBE are usually carbonate-pure and accompanied by geochemical inferences of enhanced alkalinity (higher Sr/Ca ratios and higher HREE/LREE fractionation, i.e. higher carbonate alkalinity; Caetano-Filho et al., 2019; Paula-Santos et al., 2020) compared to the carbonate rocks deposited below this interval. Also, the MIBE corresponds to a rapid excursion to a plateau of extreme and relatively stable high $\delta^{13}C_{carb}$ values (>10‰) through hundreds of meters (Uhlein et al., 2019), which is also in disagreement with a decreased DIC reservoir that would lead to a higher variability of $\delta^{13}C_{DIC}$.

We thus want to explore the possibility that the MIBE is of local extent and of long duration (i.e. spanning the 2nd-order sequence timescale in hundreds of meters in the stratigraphy, Uhlein et al., 2019), and results from a process which could have promoted a long-term isotope disequilibrium between the basin's DIC and the global atmospheric CO_2. In other words, to keep such anomalously high $\delta^{13}C_{DIC}$ values compared to coeval global seawater in the time-scale of million years, the regional carbon cycle in the Ediacaran-Cambrian Bambuí sea must have been dynamically maintained by a mechanism with a rate exceeding that of isotope equilibration between the DIC and the atmospheric CO_2, which is achieved in hundreds to thousands of years in continental water masses (e.g. Benson et al., 1996). In this case, the isotope mass balance equations used to model the steady-state global carbon cycle based on the hypothesis that ocean and atmosphere are in isotope equilibrium are not appropriate (e.g. Hayes et al., 1999; Schrag et al., 2013). We therefore revisit the hypotheses previously proposed for the mechanism responsible for the MIBE, namely (i) the increase in organic carbon burial, (ii) an increase in authigenic carbon precipitation, (iii) changes in isotope composition of the dissolved carbon input into the basin, and (iv) the methanogenesis coupled to methane loss to the atmosphere (e.g. Iyer et al., 1995; Paula-Santos et al., 2017; Uhlein et al., 2019).

In the modern carbon cycle the fluxes of carbon buried into sediments and the carbon delivered through riverine input into the oceans are three orders of magnitude lower than the exchange fluxes between the atmosphere and the oceans (less than 0.9 PgC yr^{-1} as opposed to 60 PgC yr^{-1}, respectively; Ciais et al., 2013). In contrast, the fluxes between surface ocean and marine biota, through photosynthesis and respiration, are of the same order of magnitude as those between the atmosphere and the ocean DIC reservoirs (37–50 PgC yr^{-1}; Ciais et al., 2013). On this basis, the increase in organic carbon burial and/or in authigenic carbon precipitation, and the change in the carbon isotope composition of dissolved carbon input by runoff into the basin are unlikely to explain the anomalous ^{13}C-enrichments found. Whether we consider equilibrium or disequilibrium scenarios between the Bambuí basin waters and the atmosphere, these fluxes should have been at least two to three orders of magnitude higher than the modern ones, for several million years in

order to result in homogeneously high $\delta^{13}C$ values of MIBE interval, which is very unlikely.

Additional arguments can be invoked to rule out that this possible disequilibria condition between DIC and atmosphere was caused locally by the mechanisms usually envisaged for global positive $\delta^{13}C$ anomalies. No significant increase in TOC content is observed below and through the excursion anywhere in the basin that could support the hypothesis of a locally increased organic carbon burial. In Well 1 section, TOC increases after the positive $\delta^{13}C$ excursions, so it cannot be interpreted as a cause for the ^{13}C enrichments. In addition, trace element data through the Bambuí deposits suggest that bottom waters were predominantly anoxic before and after the positive $\delta^{13}C_{carb}$ excursion, compatible with a scenario of stagnant waters in an epicontinental basin (Paula-Santos et al., 2018, 2020; Hippertt et al., 2019). This stasis in the redox state of the water column is also incompatible with a major change in the organic burial rate, in the sense that enhanced organic burial is often associated with enhanced reducing conditions, whether associated with increased bioproductivity or not. Increases in precipitation and burial of ^{13}C-depleted authigenic carbonates (e.g. Schrag et al., 2013) can also be ruled out to account for the MIBE. For the restricted setting of the Bambuí sea a ^{13}C-enriched signal caused by authigenic carbonate precipitation would require both the identification of intervals rich in authigenic carbonates with very negative $\delta^{13}C_{carb}$ and the decoupling between carbonate and organic carbon isotope signatures. No significant event of ^{13}C-depleted authigenic carbonate deposition preceding MIBE has been identified so far. Apart from cap carbonates, the intervals identified as possibly diagenetic (section 5.1) are very local and lithologically-controlled rather than basin-wide occurrences. Uhlein et al. (2019) pointed to the occurrence of framboidal pyrite in carbonate facies from the Lagoa do Jacaré Formation as an evidence of sulfate-reduction activity known to result in authigenic carbonate precipitation. However, these carbonate rocks present extreme positive $\delta^{13}C_{carb}$ values (>10‰), i.e., this unit belongs to the MIBE and cannot account for a ^{13}C-depleted authigenic precipitation event (Fig. 5). Finally, an increase in the $\delta^{13}C_{input}$ through riverine DIC to the basin has also been discussed for the MIBE (Uhlein et al., 2019). Because carbonates record the isotope composition of the DIC they precipitate from, the DIC generated through weathering on land and reaching the basin would need to present extremely positive $\delta^{13}C$ values to account for the MIBE. The values must have been even higher than those recorded in the excursion, since mixing with the water body DIC and ongoing isotopic exchange with the atmosphere would both tend to drive the $\delta^{13}C_{carb}$ to lower values.

Hence the only hypothesis we are left with is that of methanogenesis and methane loss to the atmosphere, representing an intrabasinal forcing on the carbon cycle as a result of drastic paleoenvironmental changes through the basal Bambuí Group deposition. In a scenario of basin restriction, progressive marine sulfate distillation would ultimately lead to a methanogenic environment (Paula-Santos et al., 2017). In anoxic and sulfate-depleted environments, methanogenesis may take place as an important early diagenetic metabolism (e.g. Gu et al., 2004; Birgel et al., 2015). This metabolism produces two carbon compounds with very distinct carbon isotope composition: a very ^{13}C-depleted CH_4 and a ^{13}C-enriched CO_2 (Whiticar et al., 1986). Studies in modern marine and lacustrine methanogenic environments show that methanogenic ^{13}C-enriched CO_2 can influence $\delta^{13}C_{DIC}$ from pore waters (up to +26‰; Gu et al., 2004) and in restricted settings can even influence the DIC of the overlying water column (Gu et al., 2004; Assayag et al., 2008). In the Lake Apopka, Florida (USA), the $\delta^{13}C_{DIC}$ and $\delta^{13}C_{POC}$ from the water column are as high as +13‰ and −13‰, respectively (Gu et al., 2004). ^{13}C enrichment in the DIC of water column is associated with diffusion and advection of ^{13}C-enriched CO_2 from the methanogenic-dominated sediments ($\delta^{13}C_{DIC}$ of pore waters ~+26‰), coupled with methane ebullition. Photosynthetic carbon fixation of this ^{13}C-enriched DIC results in similar enrichments in POC. It is important to note here that in this case, methane loss to the atmosphere is required, otherwise its oxidation in the water column would buffer the $\delta^{13}C_{DIC}$ variations by adding very ^{13}C-depleted CO_2 from methane oxidation. Gu et al. (2004) suggested several factors are favoring the establishment of such unusual conditions of highly ^{13}C-enriched DIC. Bottom water anoxia, limited sulfate availability and high bioproductivity lead to high rates of methanogenesis required to maintain a significant flux of methanogenic CO_2 to the water column. Shallow water environment and efficient wind mixing are favoring methane loss to the atmosphere, preventing its oxidation in the water column. Such scenario was proposed by Birgel et al. (2015) for the extreme ^{13}C enrichments found in stromatolites from Lagoa Salgada, a coastal lagoon located in SE Brazil. Although these ^{13}C enrichments are not present in the DIC today, the authors proposed that methanogenesis coupled to methane escape to the atmosphere strongly affected the DIC during times of stromatolite formation, under more arid and sulfate-limited conditions in Lagoa Salgada. Anoxic and sulfate-depleted bottom conditions associated with a shallow water column would be responsible for preventing methane oxidation in the water column and rapid escape to the atmosphere.

For the MIBE, the enhanced restriction of the Bambuí sea driven by the advance of the orogenic fronts over the basin may have led to its complete disconnection from the marginal seas and to sulfate exhaustion through bacterial sulfate reduction and pyrite burial during the deposition of the basal sequence (Fig. 11). This would have resulted in an expansion of the methanogenic zone to shallow depths within the sediment and even in the water column, increasing the methane concentration and its escape to the atmosphere. Methane escape to the atmosphere would have been favored by: (i) limited oxidation in a predominantly anoxic and sulfate-limited basin (e.g. Paula-Santos et al., 2017, 2020; Hippertt et al., 2019); (ii) a shallow chemocline, which would decrease the thickness of the methane oxidation zone (oxic layer), considering the absence of negative Ce anomalies from shallow to deep environments of the carbonate ramp (data from Januária and Arcos sections; Paula-Santos et al., 2020) (Fig. 11); and (iii) hypersalinity and decreased methane solubility, considering the high $\delta^{18}O_{carb}$ values in early diagenetic dolostones associated with the sequence boundary (Caetano-Filho et al., 2019). These favorable conditions for methane bypass to the atmosphere and the shallow chemocline would result in a surface marine DIC progressively enriched in ^{13}C by methanogenic CO_2, through mixing between the thin upper oxic layer and the thick anoxic bottom layer. In this scenario, the redox stratification attributed to the Bambuí sea would not imply a divided DIC pool. Consequently, primary organic biomass produced through photosynthesis would also present heavy carbon isotope compositions (e.g. Gu et al., 2004), represented by the coupled $\delta^{13}C_{carb}$ and $\delta^{13}C_{org}$ high values through the MIBE (Fig. 11).

Recent iron speciation data from Hippertt et al. (2019) show an increasing trend from euxinic to more ferruginous conditions through the MIBE. Although the authors assigned this redox change to the higher detrital input, and so, higher reactive Fe availability, these data also support a sulfate-limited condition during the excursion. This redox change through the MIBE may also explain the increase in total sulfur content in this interval (Uhlein et al., 2019), when higher reactive Fe availability favored precipitation of iron sulfides from previous euxinic waters. Therefore, sulfur isotope compositions and further iron speciation data are still required to put constraints on the sulfate availability through the MIBE and, most important, to test the scenario here proposed.

At the same time, methanogenesis would lead to acidic conditions due to massive CO_2 production, being therefore unfavorable for carbonate precipitation (e.g. Birgel et al., 2015). This would require some processes to buffer the seawater pH to explain microbial limestones and calcimudstones that dominate MIBE interval (Fig. 4F and G; Supplementary Table S1). One possibility would be an increase in alkalinity resulting from the marginal orogenic uplift and decreased continental weathering intensity due to higher denudation rates, therefore favoring weathering of carbonates and congruent silicate weathering. This was already inferred for middle Bambuí Group through unradiogenic

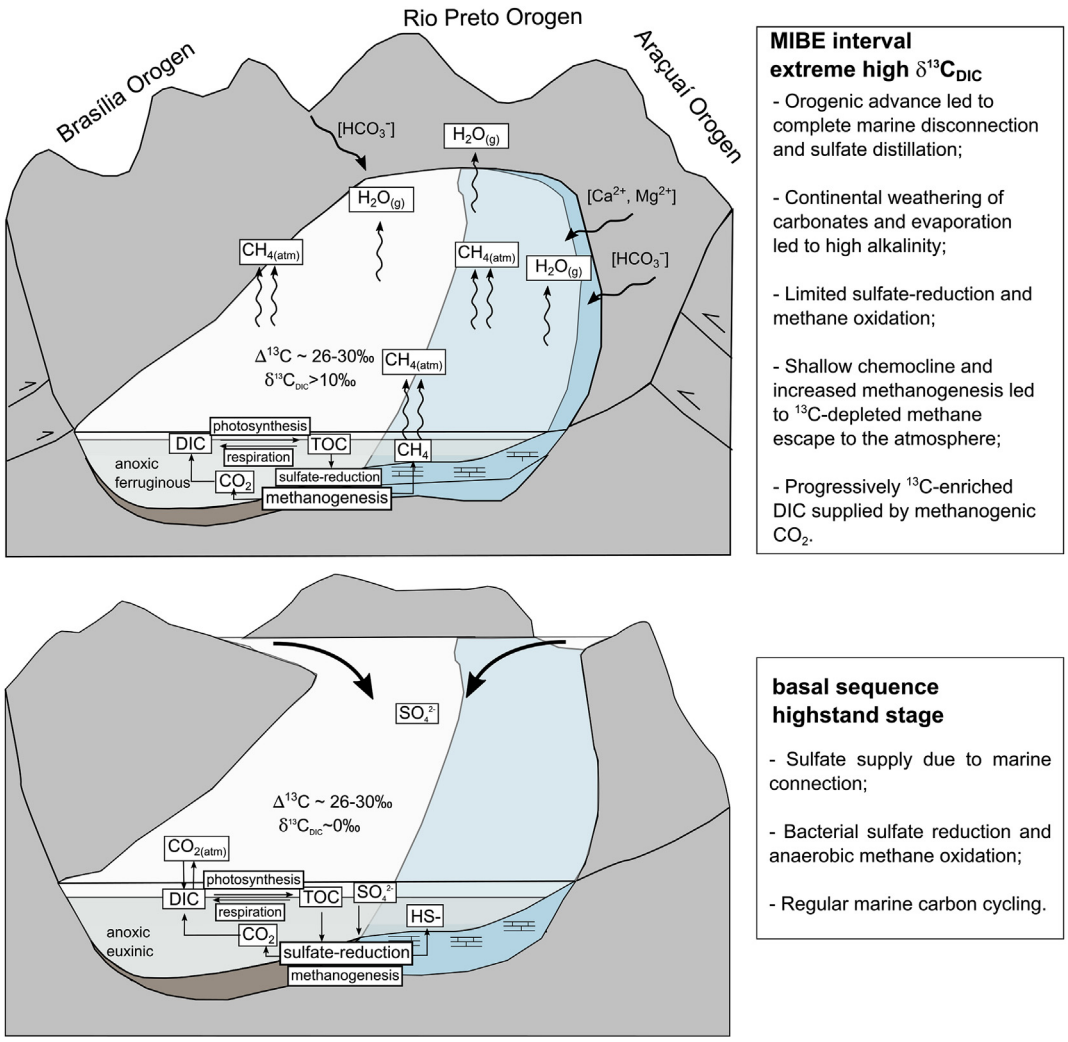

Fig. 11. Conceptual model for the marine carbon cycle disturbance between basal and overlying 2nd-order sequences from the Bambuí Group. The Middle Bambuí Excursion would represent a transition for a methanogenic dominated basin after sulfate exhaustion and limited sulfate-reduction due to orogenic build-up and marine disconnection. A shallow chemocline would decrease methane oxidation in the Bambuí sea and favor methane escape to the atmosphere (based on data from Hippertt et al., 2019 and Paula-Santos et al., 2020). A thick anoxic bottom layer would have reached photic zone in which ^{13}C-enriched methanogenic-CO^2 influenced DIC available for photosynthetic primary production, resulting in equally heavy organic and carbonate-carbon isotope compositions.

$^{87}Sr/^{86}Sr$ ratios and enhanced rare earth elements fractionation recorded in carbonates at this stage (Paula-Santos et al., 2018, 2020). In this case, sea-level fall and/or orogenic reworking and uplift would result in a large flux of ions to the basin, especially Ca^{2+} and Mg^{2+} derived from carbonate weathering (Fig. 6). Sulfate may also have been produced through oxidative weathering of pyrites and sulfate minerals from the orogens and supplied to the basin, although not in quantities large enough to counter balance a previous sulfate distillation event. Even considering a sulfate amount in the Neoproterozoic oceans 10 times lower than in the modern ocean (i.e. 1.3×10^{20} g S), a connection to the ocean would still supply much more sulfate to the Bambuí basin than the riverine sulfate input from major river systems (i.e. lower than the contemporaneous flux of 10^{14} g S yr^{-1}; Bottrell and Newton, 2006 and references therein). Therefore, a marine disconnection would critically reduce the sulfate supply to Bambuí sea. Finally, hypersalinity could also be an important factor for carbonate saturation (e.g. Birgel et al., 2015) in the scenario discussed above (Caetano-Filho et al., 2019). The isolation of the Bambuí basin in the very core of the Gondwana supercontinent might have resulted in arid conditions and negative hydrologic balance due to inefficient humidity transfer to the continent interior in times of absence of land vegetation.

5.4. *The late Ediacaran-Cambrian Gondwana basin restriction: implications for the marine environment and climate*

The extreme positive $\delta^{13}C$ anomaly from the middle Bambuí Group if associated to methanogenic environments would imply carbon isotope non-equilibrium between the marine DIC and the atmospheric CO_2 in a closed basin, resulting ultimately from the Gondwana assembly. Increased fluxes of methanogenic-derived CO_2 to the water column and methane escape to the atmosphere are combined requirements to maintain a ^{13}C-enriched DIC. Consequently, this has implications for metazoan colonization and regional climate in the West Gondwana interior during the late Ediacaran-Cambrian transition. The scenario of predominantly anoxic, sulfate-depleted, presence of free H_2S, methane-rich, and hypersaline conditions would imply in extreme environments for animal colonization (e.g. Bell, 2012; Hippertt et al., 2019). The large surface covered by the Bambuí basin (>350,000 km^2) would also represent a significant amount of methane emission to the atmosphere.

Links between the metazoan evolution and colonization and well-oxygenated environments have been extensively debated. The geochemical record of late Ediacaran successions bearing macroscopic metazoan assemblages is contradictory and points to well-oxygenated

(e.g. Tostevin et al., 2016) or to predominantly anoxic conditions (e.g. Johnston et al., 2013), with the relationship between oxygenation and animal colonization remaining unsettled (Butterfield, 2009). The paleoenvironmental changes reported here for the middle Bambuí Group seem to have prevented widespread colonization of the basin, considering the lack of macrofossils at this stage so far, and are beyond the oxygen availability discussion. More favorable conditions would have been developed in other areas where coeval basins connected to the global ocean present a rich fossil record (Corumbá Group, Southern Paraguay Belt, and Arroyo del Soldado Group, Uruguay; e.g. Gaucher et al., 2003; Nama Group; Namibia; e.g. Tostevin et al., 2016). Besides oxygen depletion, the combination of other factors that characterize extreme environments, such as the presence of toxic free-H_2S in bottom waters as a result of a possible sulfate-distillation event driven by microbial sulfate reduction, could have precluded animal colonization in the Bambuí basin during the Ediacaran-Cambrian transition (e.g. Hippertt et al., 2019). Furthermore, the large methanogenic emissions from the Bambuí basin would result in high inputs of methane to the atmosphere. If similar environments existed in West Gondwana, it would imply in huge methane inputs to the atmosphere with potential impact over the global climate dynamics in the beginning of the Phanerozoic Eon.

6. Conclusions

The paired $\delta^{13}C$ evolution for the basal Bambuí Group illustrates the particular marine carbon cycling within epicontinental settings in terminal Neoproterozoic/early Paleozoic. At the base, a cap carbonate interval shows mirrored $\delta^{13}C_{carb}$ and $\delta^{13}C_{org}$ excursions, resulting in great variation in $\Delta^{13}C$, also recorded in other Ediacaran cap carbonates and Ediacaran-Cambrian successions. Upwards, the positive $\delta^{13}C$ excursion of the middle Bambuí Group presents a coupled and basin-wide behavior, from shallower to deeper paleodepositional systems, attesting to the change in DIC isotope composition linked to the progressive foreland-related restriction of the basin at the late Ediacaran-Cambrian transition. Our results show that the classical interpretation of enhanced organic carbon burial, as well as other forcing controls (changes in $\delta^{13}C_{input}$ and fraction of authigenic carbonate buried), are unlikely to explain the extremely heavy carbon isotope compositions in a local marine carbon cycling. An intrabasinal and long-lived control may have caused significant disturbances in the marine carbon cycle in response to the West Gondwana assembly. We propose a scenario with a progressively methanogenic-dominated basin developed after a sulfate distillation event in an isolated marine setting, barred from sulfate recharge from the marginal seas. In this scenario, the extremely positive $\delta^{13}C_{DIC}$ values of Bambuí basin instead of being of global significance, would represent a regional disequilibria between atmospheric CO_2 and the DIC reservoir in a large restricted basin in the very core of West Gondwana landmass. Anoxic and sulfate depleted conditions hampered methane oxidation and, together with possibly hypersalinity and dominant shallow chemocline, allowed methane to escape to the atmosphere. This would result in ^{13}C-enriched DIC derived from methanogenic CO_2, with carbonates and primary organic matter equally enriched in ^{13}C.

Paleogeographic isolation and local paleoenvironmental conditions (anoxic, sulfate-depleted, presence of free-H_2S, methane rich, hypersaline) may have created extreme conditions and an ultimate challenge to metazoan migration and colonization of marine settings in the supercontinent interior. If reproducible in other coeval epicontinental basins, the proposed methanogenic scenario although resulting from local mechanisms, could affect the global carbon cycle and the climate system globally through an increased flux of methane to the atmosphere. Importantly, our proposed scenario is testable through different approaches, including investigations of the sulfur and iron cycles, the weathering regime, and the paleontological record of the Bambuí basin, especially throughout the whole MIBE interval, as well as in equivalent intracratonic basins within the West Gondwana. Further studies concerning these areas are required to improve the understanding of such extreme positive $\delta^{13}C$ excursions in the geological record.

Declaration of competing interest

The authors declare that they have no known competing financial interests or personal relationships that could have appeared to influence the work reported in this paper.

Acknowledgements

This study was funded by the São Paulo Research Foundation (FAPESP) thematic project grant #2016/06114-6 and Brazilian Research Council project grant #400764/2016-4. We acknowledge to Lhoist and Petra Energia S.A. for providing drill core samples, and to Pôle de Spectométrie Océan staff, University of Western Brittany, for the technical support in data acquisition. Sergio Caetano Filho holds a FAPESP scholarship grant #2016/11496-5. Gustavo M. Paula-Santos holds a FAPESP post-doc grant #2017/00399-1. Marly Babinski, Ricardo Trindade and Matheus Kuchenbecker are fellows of the Brazilian Research Council (#307563/2013-8, #206997/2014-0 and #309106/2017-6, respectively). This study contributes to the IdEx Université de Paris ANR-18-IDEX-0001 and to the LabexMER ANR-10-LABX-19. IPGP contribution N° 4103. Finally, we thank to Prof. Linda Kah and Prof. Gabriel Uhlein for their helpful and constructive reviews which improved this manuscript, and to the Prof. Richard Damian Nance for the careful editorial handling.

Appendix A. Supplementary data

Supplementary data to this article can be found online at https://doi.org/10.1016/j.gsf.2020.04.005.

References

Ader, M., Javoy, M., 1998. Diagenese précoce en milieu sulfuré réducteur: une étude isotopique dans le Jurassique basal du Bassin parisien. Comptes Rendus de l'Académie des Sciences, Paris, Sciences de la terre et des planètes 327, 803–809.

Ader, M., Macouin, M., Trindade, R.I.F., Hadrien, M.H., Yang, Z., Sun, Z., Besse, J., 2009. A multi layered water column in the Ediacaran Yangtze platform? Insights from carbonate and organic matter paired $\delta^{13}C$. Earth Planet Sci. Lett. 288, 213–227.

Alkmim, F.F., Marshak, S., Pedrosa-Soares, A.C., Peres, G.G., Cruz, S.C., Whittington, A., 2006. Kinematic evolution of the araçuaí–west Congo orogen in Brazil and africa: nutcracker tectonics during the neoproterozoic assembly of Gondwana. Precambrian Research 149, 43–63.

Amthor, J.E., Grotzinger, J.P., Schröder, S., Bowring, S.A., Ramezani, J., Martin, M.W., Matter, A., 2003. Extinction of *Cloudina* and *namacalathus* at the precambrian-cambrian boundary in Oman. Geology 31, 431–434.

Assayag, N., Jezequel, D., Ader, M., Michard, G., Viollier, E., Prevot, F., Agrinier, P., 2008. Hydrological budget, carbon sources and biogeochemical processes in Lac Pavin (France): constraints from $\delta^{18}O$ and $\delta^{13}C$ of dissolved inorganic carbon. Appl. Geochem. 23 (10), 2800–2816.

Babinski, M., Vieira, L.C., Trindade, R.I.F., 2007. Direct dating of the Sete Lagoas cap carbonate (Bambuí Group, Brazil) and implications for the Neoproterozoic glacial events. Terra. Nova 19, 401–406.

Bartley, J.K., Kah, L.C., 2004. Marine carbon reservoir, C_{org}-C_{carb} coupling, and the evolution of the Proterozoic carbon cycle. Geology 32 (2), 129–132.

Bell, E., 2012. Life at Extremes: Environments, Organisms and Strategies for Survival. CABI, Wallingford, p. 576.

Benson, L., White, L.D., Rye, R., 1996. Carbonate deposition, Pyramid Lake Subbasin, Nevada: 4. Comparison of the stable isotope values of carbonate deposits (tufas) and the Lahontan lake-level record. Palaeogeogr. Palaeoclimatol. Palaeoecol. 122, 45–76.

Birgel, D., Meister, P., Lundberg, R., Horath, T.D., Bontognali, T.R.R., Bahniuk, A.M., Rezende, C.E., Vasconcelos, C., McKenzie, J.A., 2015. Methanogenesis produces strong 13C enrichment in stromatolites of Lagoa Salgada, Brazil: a modern analogue for Paleo-/Neoproterozoic stromatolites? Geobiology 13, 245–266.

Boggiani, P.C., Gaucher, C., Sial, A.N., Babinski, M., Simon, C.M., Riccomini, C., Ferreira, V.P., Fairchild, T.R., 2010. Chemostratigraphy of the tamengo formation (corumbá group, Brazil): a contribution to the calibration of the ediacaran carbon-isotope curve. Precambrian Research 182, 382–401.

Bottrell, S.H., Newton, R.J., 2006. Reconstruction of changes in global sulfur cycling from marine sulfate isotopes. Earth Sci. Rev. 75, 59–83.

Butterfield, N.J., 2009. Oxygen, animals and oceanic ventilation: an alternative view. Geobiology 7, 1–7.

Caetano-Filho, S., Paula-Santos, G.M., Guacaneme, C., Babinski, M., Bedoya-Rueda, C., Peloso, M., Amorim, K., Afonso, J., Kuchenbecker, M., Reis, H.L.S., Trindade, R.I.F., 2019. Sequence stratigraphy and chemostratigraphy of an Ediacaran-Cambrian

foreland-related carbonate ramp (Bambuí Group, Brazil). Precambrian Research 331, 105365.

Caxito, F.A., Frei, R., Uhlein, G.J., Dias, T.G., Árting, T.B., Uhlein, A., 2018. Multiproxy geochemical and isotope stratigraphy records of a neoproterozoic oxygenation event in the ediacaran Sete Lagoas cap carbonate, Bambuí group, Brazil. Chem. Geol. 481, 119–132.

Ciais, P., Sabine, C., Bala, G., Bopp, L., Brovkin, V., Canadell, J., Chhabra, A., DeFries, R., Galloway, J., Heimann, M., Jones, C., Le Quéré, C., Myneni, R.B., Piao, S., Thornton, P., 2013. Carbon and other biogeochemical cycles. In: Stocker, T.F., Qin, D., Plattner, G.-K., Tignor, M., Allen, S.K., Boschung, J., Nauels, A., Xia, Y., Bex, V., Midgley, P.M. (Eds.), Climate Change 2013: the Physical Science Basis. Contribution of Working Group I to the Fifth Assessment Report of the Intergovernmental Panel on Climate Change. Cambridge University Press, Cambridge, United Kingdom and New York, NY, USA, p. 106.

Crockford, P.W., Wing, B.A., Paytan Hodgskiss, M.S.W., Mayfield, K.K., Hayles, J.A., Middleton, J.E., Ahm, A.S.C., Johnston, D.T., Caxito, F., Uhlein, G.J., Halverson, G.P., Eickmann, B., Torres, M., Horner, T.J., 2019. Barium-isotopic constraints on the origin of post-Marinoan barites. Earth Planet Sci. Lett. 519, 234–244.

Cui, H., Kaufman, A.J., Peng, Y., Liu, X.M., Plummer, R.E., Lee, E.I., 2018. The Neoproterozoic Hüttenberg $\delta^{13}C$ anomaly: genesis and global implications. Precambrian Research 313, 242–262.

Derry, L.A., 2010. A burial diagenesis origin for the Ediacaran Shuram–Wonoka carbon isotope anomaly. Earth Planet Sci. Lett. 294 (1–2), 152–162.

Fanton, K.C., Holmden, C., 2007. Sea-level forcing of carbon isotope excursions in epeiric seas: implications for chemostratigraphy. Can. J. Earth Sci. 44, 807–818.

Fike, D.A., Grotzinger, J.P., 2008. A paired sulfate-pyrite $\delta^{34}S$ approach to understanding the evolution of the Ediacaran–Cambrian sulfur cycle. Geochem. Cosmochim. Acta 72, 2636–2648.

Galimov, E.M., 2004. The pattern of δ13Corg versus HI/OI relation in recent sediments as an indicator of geochemical regime in marine basins: comparison of the Black Sea, Kara Sea, and Cariaco Trench. Chem. Geol. 204, 287–301.

Gaucher, C., Boggiani, P.C., Sprechmann, P., Sial, A.N., Fairchild, T.R., 2003. Integrated correlation of the Vendian to Cambrian Arroyo del Soldado and Corumbá groups (Uruguay and Brazil): palaeogeographic, palaeoclimatic and palaeobiologic implications. Precambrian Research 120, 241–278.

Geyman, E.C., Maloof, A.C., 2019. A diurnal carbon engine explains ^{13}C-enriched carbonates without increasing the global production of oxygen. Proc. Natl. Acad. Sci. Unit. States Am. 116 (49), 24433–24439.

Grotzinger, J.P., Waters, W.A., Knoll, A.H., 2000. Calcified metazoans in thrombolite stromatolite reefs of the terminal Proterozoic Nama Group, Namibia. Paleobiology 26 (3), 334–359.

Gu, B., Schelske, C.L., Hodell, D.A., 2004. Extreme 13C enrichments in a shallow hypereutrophic lake: implications for carbon cycling. Limnol. Oceanogr. 49, 1152–1159.

Halverson, G., Hoffman, P., Schrag, D., Maloof, A., Rice, A., 2005. Towards a Neoproterozoic composite carbon isotope record. Geol. Soc. Am. Bull. 117, 1181–1207.

Halverson, G.P., Hurtgen, M.T., Porter, S.M., Collins, A.S., 2009. Chapter 10 Neoproterozoic-Cambrian Biogeochemical Evolution, Developments in Precambrian Geology. Elsevier. https://doi.org/10.1016/S0166-2635(09)01625-9.

Halverson, G.P., Wade, B.P., Hurtgen, M.T., Barovich, K.M., 2010. Neoproterozoic chemostratigraphy. Precambrian Research 182 (4), 337–350.

Hayes, J.M., Strauss, H., Kaufman, A.J., 1999. The abundance of 13C in marine organic matter and isotopic fractionation in the global biogeochemical cycle of carbon during the past 800 Ma. Chem. Geol. 161, 103–125.

Heilbron, M., Cordani, U.G., Alkmim, F.F., 2017. São Francisco Craton, Eastern Brazil: Tectonic Genealogy of a Miniature Continent. Springer, Switzerland, p. 331p.

Hippertt, J.P., Caxito, F.A., Uhlein, G.J., Nalini, H.A., Sial, A.N., Abreu, A.T., Nogueira, L.B., 2019. The fate of a Neoproterozoic intracratonic marine basin: trace elements, TOC and IRON speciation geochemistry of the Bambuí Basin. Brazil. Precambrian Res. 330, 101–120.

Iyer, S.S., Babinski, M., Krouse, H.L., Chemale, F., 1995. Highly 13C enriched carbonate and organic matter in the Neoproterozoic sediments of the Bambuí Group, Brazil. Precambrian Research 73, 271–282.

Jacobsen, S.B., Kaufman, A.J., 1999. The Sr, C and O isotopic evolution of Neoproterozoic seawater. Chem. Geol. 161, 37–57.

Jiang, G.Q., Wang, X.Q., Shi, X.Y., Zhang, S.H., Xiao, S.H., Dong, J., 2010. Organic carbon isotope constraints on the dissolved organic carbon (DOC) reservoir at the Cryogenian-Ediacaran transition. Earth Planet Sci. Lett. 299, 159–168.

Jiang, G., Wang, X., Shi, X., Xiao, S., Zhang, S., Dong, J., 2012. The origin of decoupled carbonate and organic carbon isotope signatures in the early Cambrian (ca. 542–520 Ma) Yangtze platform. Earth Planet Sci. Lett. 317–318, 96–110.

Johnston, D.T., Poulton, S.W., Tosca, N.J., O'Brien, T., Halverson, G.P., Schrag, D.P., Macdonald, F.A., 2013. Searching for an oxygenation event in the fossiliferous Ediacaran of northwestern Canada. Chem. Geol. 362, 273–286.

Knauth, L.P., Kennedy, M.J., 2009. The late Precambrian greening of the Earth. Nature 460, 728–732.

Kuchenbecker, M., Babinski, M., Pedrosa-Soares, A.C., Lopes-Silva, L., Pimenta, F., 2016. Chemostratigraphy of the lower Bambuí group, southwestern São Francisco craton, Brazil: insights on Gondwana paleoenvironments. Braz. J. Genet. 46 (1), 145–162.

Lehmann, M.F., Bernasconi, S.M., Barbieri, A., Mckenzie, J.A., 2002. Preservation of organic matter and alteration of its carbon and nitrogen isotope composition during simulated and in situ early sedimentary diagenesis. Geochem. Cosmochim. Acta 66, 3573–3584.

Macko, S.A., Engel, M.H., Qian, Y., 1994. Early diagenesis and organic matter preservation – a molecular stable carbon isotope perspective. Chem. Geol. 114, 365–379.

McKirdy, D.M., Powell, T.G., 1974. Metamorphic alteration of carbon isotopic composition in ancient sedimentary organic matter: new evidence from Australia and South Africa. Geology 2, 591–595.

Och, L.M., Shields-Zhou, G.A., 2012. The Neoproterozoic oxygenation event: environmental perturbations and biogeochemical cycling. Earth Sci. Rev. 110, 26–57.

Okubo, J., Muscente, A.D., Luvizotto, G.L., Uhlein, G.J., Warren, L.V., 2018. Phosphogenesis, aragonite fan formation and seafloor environments following the Marinoan glaciation. Precambrian Research 311, 24–36.

Pasquier, V., Sansjofre, P., Lebeau, O., Liorzou, C., Rabineau, M., 2018. Acid digestion on river influenced shelf sediment organic matter: carbon and Nitrogen contents and isotopic ratios. Rapid Commun. Mass Spectrom. 32, 86–92.

Paula-Santos, G.M., Babinski, M., Kuchenbecker, M., Caetano-Filho, S., Trindade, R.I.F., Pedrosa-Soares, A.C., 2015. New evidence of an Ediacaran age for the Bambuí Group in southern São Francisco craton (eastern Brazil) from zircon U-Pb data and isotope chemostratigraphy. Gondwana Research 28, 702–720.

Paula-Santos, G.M., Caetano-Filho, S., Babinski, B., Enzweiler, J., 2018. Rare earth elements of carbonate rocks from the Bambuí Group, southern São Francisco Basin, Brazil, and their significance as paleoenvironmental proxies. Precambrian Research 305, 327–340.

Paula-Santos, G.M., Caetano-Filho, S., Babinski, M., Trindade, R.I.F., Guacaneme, C., 2017. Tracking connection and restriction of West Gondwana São Francisco basin through isotope chemostratigraphy. Gondwana Research 42, 280–305.

Paula-Santos, G., Caetano-Filho, S., Enzweiler, J., Navarro, M., Babinski, M., Guacaneme, C., Kuchenbecker, M., Reis, H., Trindade, R.I.F., 2020. Rare earth elements in the terminal Ediacaran Bambuí Group carbonate rocks (Brazil): evidence for high seawater alkalinity during rise of early animals. Precambrian Research 336, 105506.

Perrella Jr., Uhlein, Uhlein, Sial, Pedrosa-Soares, Lima, 2017. Facies analysis, sequence stratigraphy and chemostratigraphy of the Sete Lagoas Formation (Bambuí Group), northern Minas Gerais State, Brazil: evidence of a cap carbonate deposited on the Januária basement high. Brazilian Journal of Geology 47, 59–77. https://doi.org/10.1590/2317-4889201720160112.

Reis, Alkmim, 2015. Anatomy of a basin-controlled foreland fold-thrust belt curve: the Três Marias salient, São Francisco basin, Brazil. Marine Petroleum Geology. Marine Petroleum Geology 66 (4), 711–731.

Reis, H.L.S., Alkmim, F.F., Fonseca, R.C.S., Nascimento, T.C., Suss, J.F., Prevatti, L.D., 2016. The São Francisco basin. In: Heilbron, M., Cordani, U.G., Alkmim, F.F. (Eds.), São Francisco Craton, Eastern Brazil, Regional Geology Reviews. Springer, Switzerland, pp. 117–143.

Reis, H.L.S., Suss, J.F., 2016. Mixed carbonate-siliciclastic sedimentation in forebulge grabens: an example from the ediacaran Bambuí group, São Francisco basin, Brazil. Sediment. Geol. 339, 83–103.

Reis, H.L.S., Suss, J.F., Fonseca, R.C.S., Alkmim, F.F., 2017. Ediacaran forebulge grabens of the southern São Francisco basin, SE Brazil: craton interior dynamics during West Gondwana assembly. Precambrian Research 302, 150–170.

Rothman, D.H., Hayes, J.M., Summons, R.E., 2003. Dynamics of the Neoproterozoic carbon cycle. Proc. Natl. Acad. Sci. U.S.A. 100 (14), 8124–8129.

Sansjofre, P., Ader, M., Trindade, R.I.F., Elie, M., Lyons, J., Cartigny, P., Nogueira, A.C.R., 2011. A carbon isotope challenge to the snowball Earth. Nature 478, 93–96.

Santos, R.V., Alvarenga, C.J.S., Babinski, M., Ramos, M.L.S., Cukrov, N., Fonseca, M.A., Sial, A.N., Dardenne, M.A., Noce, C.M., 2004. Carbon isotopes of mesoproterozoic-neoproterozoic sequences from southern São Francisco craton and araçuaí belt, Brazil: paleogeographic implications. J. S. Am. Earth Sci. 18, 27–39.

Schrag, D.P., Higgins, J.A., Macdonald, F.A., Johnston, D.T., 2013. Authigenic carbonate and the history of the global carbon cycle : why diagenesis matters even more. Sci. Adv. 339, 2223.

Simoneit, B.R.T., Peters, K.E., Rohrback, B.G., Brenner, S., Kaplan, I.R., 2004. Thermal alteration of cretaceous black shale from the eastern atlantic. III: laboratory simulations. In: Hill, R.J., Leventhal, J., Aizenshtat, Z., Baedecker, M.J., Claypool, G., Eganhouse, R., Goldhaber, M., Peters, K. (Eds.), Geochemical Investigations in Earth and Space Science: A Tribute to Isaac R. Kaplan, vol. 9. The Geochemical Society No., pp. 321–340

Swart, P.K., 2008. Global synchronous changes in the carbon isotopic composition of carbonate sediments unrelated to changes in the global carbon cycle. Proc. Natl. Acad. Sci. Unit. States Am. 105 (37), 13741–13745.

Tohver, E., D'Agrella Filho, M.S., Trindade, R.I.F., 2006. Paleomagnetic record of africa and South America for the 1200-500 Ma interval, and evaluation of rodinia and Gondwana assemblies. Precambrian Research 147, 193–222.

Tostevin, R., Wood, R.A., Shields, G.A., Poulton, S.W., Guilbaud, R., Bowyer, F., Penny, A.M., He, T., Curtis, A., Hoffmann, K.H., Clarkson, M.O., 2016. Low-oxygen waters limited habitable space for early animals. Nat. Commun. 7, 1–9.

Uhlein, G.J., Uhlein, A., Pereira, E., Caxito, F.A., Okubo, J., Warren, L.V., Sial, A.N., 2019. Ediacaran paleoenvironmental changes recorded in the mixed carbonate-siliciclastic Bambuí Basin, Brazil. Palaeogeogr. Palaeoclimatol. Palaeoecol. 517, 39–51.

Vieira, L.C., Trindade, R.I.F., Nogueira, A.C.R., Ader, M., 2007. Identification of a sturtian cap carbonate in the neoproterozoic Sete Lagoas carbonate plataform, Bambuí group, Brazil. Compt. Rendus Geosci. 339, 240–258.

Warren, L.V., Quaglio, F., Riccomini, C., Simões, M.G., Poiré, D.G., Strikis, N.M., Anelli, L.E., Strikis, P.C., 2014. The puzzle assembled: Ediacaran guide fossil Cloudina reveals an old proto-Gondwana seaway. Geology 42 (5), 391–394.

Whiticar, M.J., Faber, E., Schoell, M., 1986. Biogenic methane formation in marine and freshwater environments: CO2 reduction versus acetate fermentation? Isotope evidence. Geochem. Cosmochim. Acta 50, 693–709.

Yamaguchi, K.E., Oguri, K., Ogawa, N.O., Sakai, S., Hirano, S., Kitazato, H., Ohkouchi, N., 2010. Geochemistry of modern carbonaceous sediments overlain by a water mass showing photic zone anoxia in the saline meromictic Lake Kai-ike, southwest Japan: I. Early diagenesis of organic carbon, nitrogen, and phosphorus. Palaeogeogr. Palaeoclimatol. Palaeoecol. 294, 72–82.

Zhou, C., Xiao, S., 2007. Ediacaran $\delta^{13}C$ chemostratigraphy of South China. Chem. Geol. 237, 89–108.